Chemical Fueling Enables Molecular Complexification of Assembly-Driven Self-Replicators

Shuo Yang[1], Gael Schaeffer[1], Elio Mattia[1], Omer Markovitch[1,2], Kai Liu[1],Andreas S. Hussain[1], Jim Ottelé[1], Ankush Sood[1], Sijbren Otto[1,*]

Affiliations:

[1]Centre for Systems Chemistry, Stratingh Institute, University of Groningen, Nijenborgh 4, 9747 AG Groningen, the Netherlands.

[2] Origins Center, Nijenborgh 7, 9747 AG, Groningen, The Netherlands.

*Correspondence to: s.otto@rug.nl.

Life can be considered as an emergent property of a highly complex chemical system. Establishing how chemical systems can complexify to the point that life emerges is among the grand challenges in contemporary science. In the different approaches to this question[1,2,3,4], self-replicating systems[5,6,7,8,9] play an essential role. The heritability associated with self-replicating systems enables Darwinian evolution[10,11] which is a powerful mechanism for complexification. However, in many experiments on the evolution of replicators the opposite was observed: replicators have a tendency to become smaller as smaller replicators tend to be replicated faster[12,13,14,15]. Here we show that, when a system of replicators is subjected to a regime where replication competes with replicator destruction, simple and fast replicators can give way to more complex and slower ones. The structurally more complex replicator was found to be functionally more proficient in the catalysis of a model reaction. These results show that chemical fueling can maintain systems of replicators out of equilibrium, populating more complex replicators that are otherwise not readily accessible. Such complexification represents an important requirement for achieving open-ended evolution as it should allow improved and ultimately also new functions to emerge.

The transitions from non-living matter to primitive life to evolved life are associated with an increase in molecular complexity and ordering. Producing a state of local ordering is entropically costly and can only occur if it is coupled to and accompanied by a larger increase in the entropy of the surroundings. A living organism is able to reach and maintain its complex entropically disfavored and far-from-equilibrium state by coupling its internal organization to chemical processes that are producing entropy externally, like the burning of a fuel. Inspired by this mechanism, we reasoned that the chemical fueling of a process of self-replication should enable the molecular complexification of the replicator. Chemical fueling has been utilized to achieve dissipative self-assembly[16,17,18,19,20,21,22,23], to drive micellization-driven physical autocatalystst out of equilibrium[24] and to create bistability in replicator networks[25]. No molecular complexification was observed in these fueled systems. Chemically fueled replication may be implemented by creating a regime in which replicator formation competes with replicator destruction and at least one of these processes is driven by a high-energy reactant. We decided to test this important concept of fueled molecular complexification using a system of fully synthetic replicators (i.e. unconstrained by canonical

biochemistry or considerations of prebiotic relevance). We previously reported a system of self-assembly driven self-replication [26, 27, 28, 29] that could potentially be subjected to a chemically fueled replication-destruction regime. In brief, oxidation of dithiol building block **1** yields a mixture of disulfides of different ring sizes that interconvert through disulfide exchange[30]. If rings of a specific size are able to self-assemble by stacking into fibers, this stabilizes this ring and the composition will change to produce more of the very ring that assembles, resulting in self-replication (Figure 1A). Mechanically induced breakage of the fibers increases the number of ends from which the fibers grow, enabling exponential growth[28] of the replicator. We now report that chemically fueling a system in which two differently sized replicators compete for a common building block results in the population of the replicator with the highest molecular complexity[31,32], even though the more complex replicator replicates slower than its competitor.

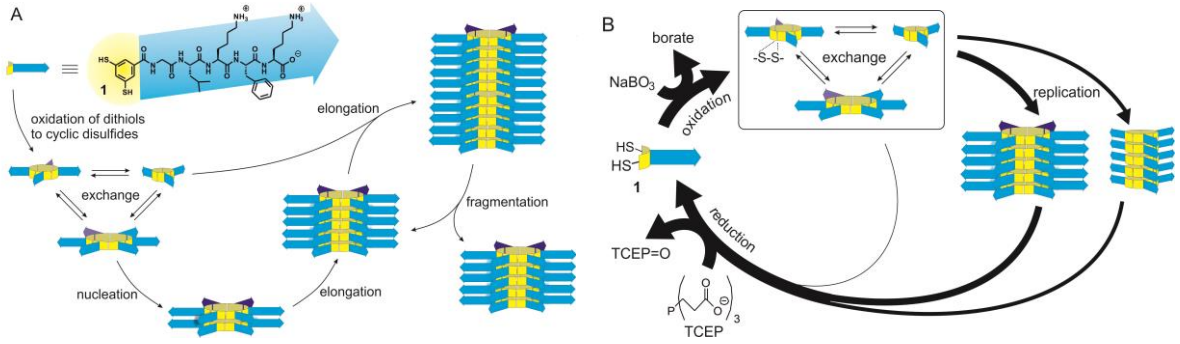

Fig. 1. Schematic representation of assembly-driven self-replication in replication-destruction regime. (A) Mechanism of self-replication. Dithiol building block **1** is oxidized to give rise to a mixture of interconverting disulfides of different ring size. Slow nucleation of a stack of one particular ring size is followed by elongation of the stack. When the stack is sufficiently long to be susceptible to mechanical energy the system enters a breakage-elongation cycle leading to exponential growth of the fibers and the macrocycles from which they are constituted. (B) Simplified representation of the replication-destruction regime achieved upon constant simultaneous addition of oxidant and reductant. $NaBO_3$ oxidizes the dithiol building block into a mixture of different disulfide macrocycles, from which two competing replicators can grow. TCEP reduces the disulfides in the non-assembled macrocycles as well as in the assembled replicating macrocycles back to the thiol building block. The thickness of the arrows indicate the magnitude of the fluxes (in units of **1**) through the various pathways in a kinetic model of the reaction network (Supporting Information Section S4). The flux through the short-circuiting reaction of perborate with TCEP (not shown) accounts for less than 0.1% of the total flux.

Comparing the replication rate and thermodynamic stability of replicators $\mathbf{1_3}$ and $\mathbf{1_6}$

We discovered that building block **1**, when oxidized by oxygen from the air in the presence of guanidinium chloride, gives rise to self-replicating cyclic trimers. Their spontaneous emergence from a mixture of interconverting macrocycles was monitored over time using ultra performance liquid chromatography (UPLC) analysis (Figure 2A). Analysis by transmission electron microscopy (TEM) revealed that $\mathbf{1}_3$ assembled into fibrous aggregates (Figure 2B). The autocatalytic nature of the replication process was confirmed by seeding the

sample with various amounts of trimer, which was found to accelerate trimer production (Figure 2C and Supporting Information Figure S4A-C).

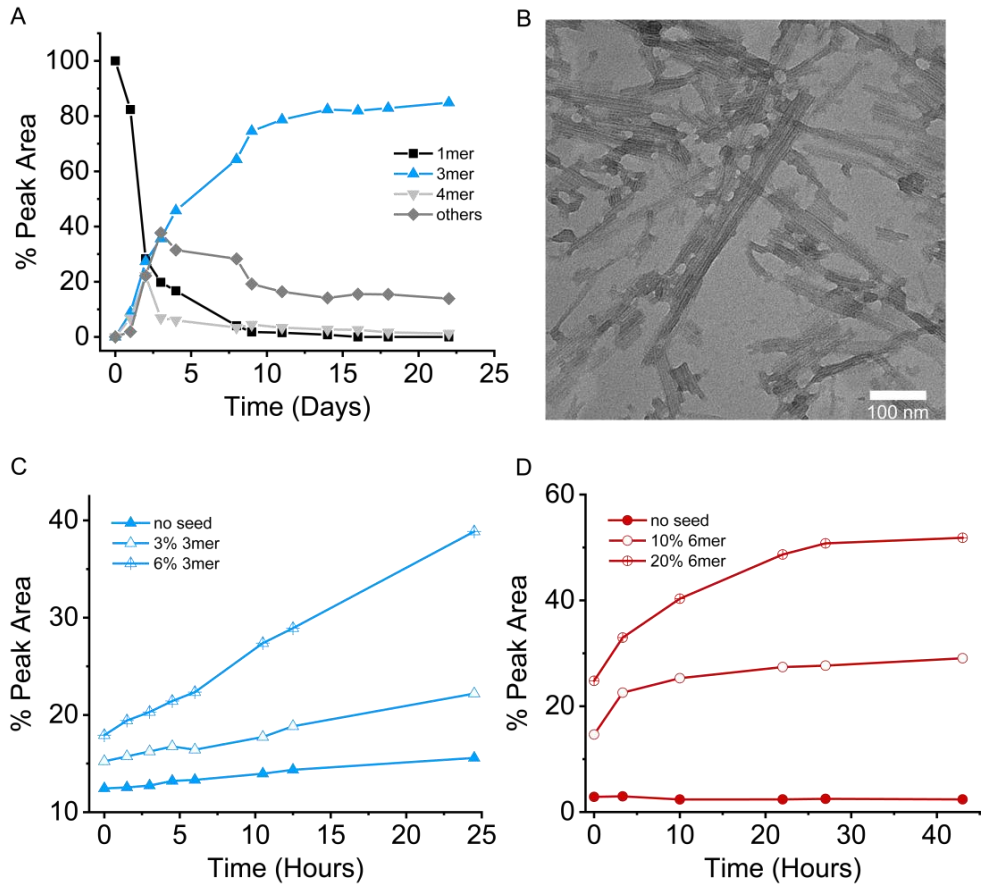

Fig. 2. Self-assembly driven self-replication of $\mathbf{1}_3$ and $\mathbf{1}_6$. (A) Change in product distribution with time of a mixture made from dithiol building block **1** (0.19 mM) in borate buffer (pH 8.2) in the presence of 2.5 M guanidinium chloride; (B) TEM analysis of the mixture dominated by trimers (scale bar = 100 nm); Change in product distribution with time of a pre-oxidized sample made from **1** (0.19 mM) in borate buffer pH 8.2 in the presence of 1.5 M guanidinium chloride in the absence and presence of various initial amounts of seeds of (C) $\mathbf{1}_3$ replicator and (D) $\mathbf{1}_6$ replicator. Seeding % are expressed in units of **1** relative to the total number of units of **1.** Lines are drawn to guide the eye.

This system was an attractive candidate to target fueling-driven replicator complexification, as previous work has shown that building block **1**, in the absence of guanidinium chloride, gives rise to a more complex replicator, featuring larger six-membered rings ($\mathbf{1}_6$)[27]. We confirmed through seeding experiments that the latter was also able to replicate in the presence of 1.5 M guanidinium chloride (Figure 2D and Supporting Information Figure S4B), albeit less efficiently than in the absence of guanidinium chloride[27]. We tentatively ascribe this impediment of hexamer replication to the known tendency of guanidinium chloride to disrupt the secondary structure of proteins. This explanation was supported by thioflavin T fluorescence experiments which showed that guanidinium chloride diminished the extent of β-sheet formation in hexamer stacks, which is one of the driving forces for the assembly of hexamers into fibers (see Supporting Information Figure S5). Note that UPLC peak areas can be used to quantify the relative amounts of **1** in the different replicators since the molar

absorptivity of a unit of **1** was found to be independent of the ring in which it resides (Supporting Information Figure S6).

The rate of replication of $\mathbf{1}_6$ in the presence of guanidinium chloride was smaller than that of $\mathbf{1}_3$. This difference was evident from experiments in which both replicators competed for common resources in the presence of oxygen from the air (Figure 3A), where trimer replicator dominated. We also compared the rate of replication of trimers and hexamers separately by mixing pre-formed replicator with monomer **1**, immediately followed by adding perborate (the oxidant used in the fueled replication regime; vide infra). The trimer replicator was able to consume essentially all the monomer before oxidation was complete (whereupon replication halts), while the hexamer replicator did so only partially (Supporting Information Figure S1). Thus, the activation barrier that separates the building blocks from the replicator is higher for replicator $\mathbf{1}_6$ than for $\mathbf{1}_3$ (i.e. $\Delta G^{\ddagger}_{ox,\mathbf{1}(6)} > \Delta G^{\ddagger}_{ox,\mathbf{1}(3)}$ as shown qualitatively in Figure 4A). Replicator $\mathbf{1}_3$ is also likely to be thermodynamically more stable than $\mathbf{1}_6$, evident from the fact that when both replicators compete for common resources, in the absence of chemical fueling, $\mathbf{1}_3$ grows where $\mathbf{1}_6$ diminishes (Figure 3B). The corresponding lower Gibbs energy of $\mathbf{1}_3$ compared to $\mathbf{1}_6$ is also shown in Figure 4A. Note that in this analysis we assume that the mechanical energy provided by stirring does not impact on the relative thermodynamic stabilities of the self-replicators (exchange experiments in the absence of agitation were precluded as isotopic labelling experiments, conducted previously, indicate that material in hexamer fibers is kinetically trapped under these conditions[33]). Thus, $\mathbf{1}_6$ is both a slower replicator and appears to be thermodynamically less stable than $\mathbf{1}_3$. Populating this replicator under conditions in which only replicator formation takes place (the experimental regime used in the vast majority of studies on self-replication) is impossible. Yet, populating $\mathbf{1}_6$ should become feasible in a regime in which both replicator formation and destruction take place, provided that the destruction of $\mathbf{1}_3$ is faster than the destruction of $\mathbf{1}_6$.

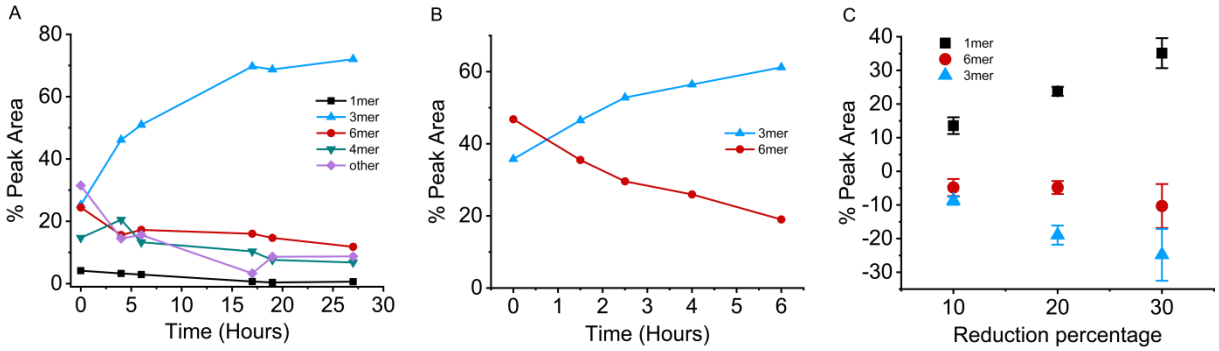

Fig. 3: Comparison of reactivity and thermodynamic stability of replicators $\mathbf{1}_3$ and $\mathbf{1}_6$. (A) In a mixture of replicators $\mathbf{1}_3$ and $\mathbf{1}_6$ and non-assembled $\mathbf{1}_3$ and $\mathbf{1}_4$ macrocycles (in a 15:30:55 ratio in units of building block) $\mathbf{1}_3$ replicates faster than $\mathbf{1}_6$. The 0.50 mL sample was shaken at 1200 rpm in the presence of oxygen from the air. (B) Change in product distribution with time of a mixture made from replicators $\mathbf{1}_3$ and $\mathbf{1}_6$ (approximately equimolar in units of **1**) in 1.5 M guanidinium chloride in the presence of 5.0 mol% dithiol **1**. Total [**1**] = 0.19 mM. (C) Decrease in UPLC peak area of replicators $\mathbf{1}_3$ (blue triangles) and $\mathbf{1}_6$ (red circles) and corresponding increase in peak area of monomer **1** (black squares) upon reduction of a mixture of these replicators (0.095 mM each in units of building block **1**) to different extents by adding 8, 20 or 40 mol% TCEP (with respect to units of **1**). Error bars show the standard deviations of three independent repeats. All samples were prepared in borate buffer (50 mM,

pH 8.2) containing 1.5 M guanidinium chloride. Lines in panels A and B are drawn to guide the eye.

Molecular complexification in a chemically fueled replication-destruction cycle

A destruction reaction was readily implementable since disulfide bonds can be reduced cleanly to thiols using tricarboxyethylphosphine (TCEP; Figure 1B). We investigated the relative rate of destruction of replicators $\mathbf{1}_3$ and $\mathbf{1}_6$ in a competition experiment in which equimolar amounts of $\mathbf{1}_3$ and $\mathbf{1}_6$ were subjected to increasing concentrations of TCEP. The results (Figure 3C) show that $\mathbf{1}_3$ is indeed more rapidly reduced than $\mathbf{1}_6$. Thus, the kinetic barrier for reduction of $\mathbf{1}_6$ is higher than that for the reduction of $\mathbf{1}_3$ as shown qualitatively in Figure 4A ($\Delta G^{\ddagger}_{\mathrm{rd},\mathbf{1}(6)} > \Delta G^{\ddagger}_{\mathrm{rd},\mathbf{1}(3)}$).

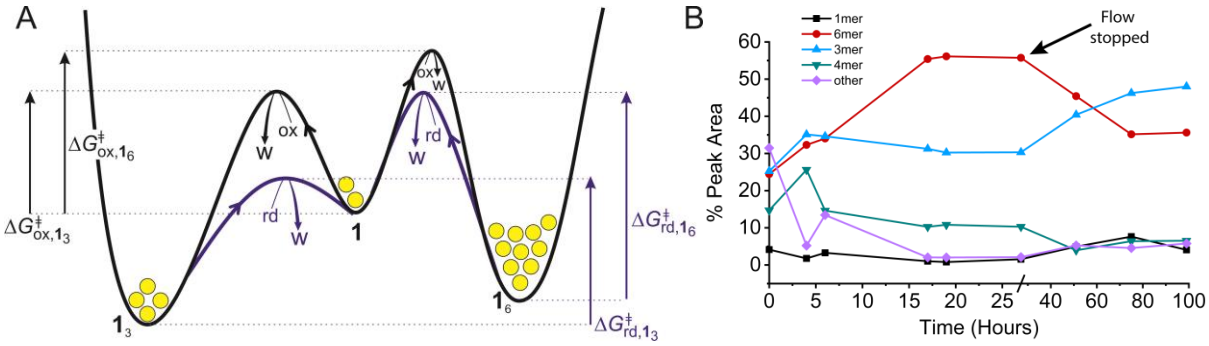

Fig. 4: Population of a thermodynamically disfavored and slow replicator is possible in a chemically fueled replication-destruction regime. (A) Potential energy landscape in which replicators $\mathbf{1}_3$ and $\mathbf{1}_6$ compete for building block **1** qualitatively showing the energy barriers for the replication (black line) and destruction (blue line) pathways. The formation of each replicator from building block **1** is coupled to the conversion of oxidant (ox) into waste (w), while the disassembly of replicators back into building block is coupled to the conversion of reducing agent (rd) into waste. (B) Evolution of the product distribution with time upon continuous and simultaneous addition of TCEP and $NaBO_3$ solutions to a mixture initially containing replicators $\mathbf{1}_3$ and $\mathbf{1}_6$ and non-assembled **1**, $\mathbf{1}_3$ and $\mathbf{1}_4$ (overall 0.19 mM in **1**) in 50 mM borate buffer (pH 8.2) containing 1.5 M guanidinium chloride. The black arrow indicates the moment that the inflow of $NaBO_3$ was stopped. Lines are drawn to guide the eye. Five repeats of this experiment show that the behavior is qualitatively reproducible (see Supporting Information (Figure S2).

An important advantage of destroying the replicator by reduction is that this reaction re-generates block **1** from which the replicator originated. This characteristic allowed us to design a protocol in which an oxidation/replication process takes place concurrently with TCEP mediated replicator destruction. As oxidation mediated by oxygen from the air is relatively slow, we used sodium perborate ($NaBO_3$) as oxidant instead. Hence, the continuous additions of oxidant and reductant should result in a replication-destruction system in which the building block of the replicator is continuously recycled (Figure 1B). Note that the process of formation of the replicators from building block **1** (through the non-assembled $\mathbf{1}_3$ and $\mathbf{1}_4$ as intermediates) and their subsequent destruction back into the same building block are

mediated by specific reactants (perborate and TCEP, respectively). This process is therefore not an equilibrium reaction, but rather an out-of-equilibrium chemical cycle, fueled by oxidant and reductant (see Figure 1B).

The resulting replication-destruction system contains several competing reduction and oxidation pathways. In order for the fuels (i.e. perborate and TCEP) to be coupled to the replication process it is essential that the replicators are continuously formed and broken down. Yet competing pathways exist in which perborate and TCEP mediate the formation and cleavage of non-replicating disulfide rings (mostly non-assembled $\mathbf{1}_3$ and $\mathbf{1}_4$) or in which the two fuels react directly with each other. In order to assess the relative contributions of these competing pathways we developed a kinetic model. First, we determined the majority of the involved rate constants and reaction orders experimentally, including the rates of perborate-mediated thiol oxidation and TCEP-mediated disulfide reduction, as well as the rate of the short-circuiting reaction between perborate and TCEP and the selectivity of the oxidant and reductant in producing and consuming replicator (relative to producing/consuming the non-assembling macrocycles). We also determined the kinetic order in the different reactants. Details are provided in Supporting Information Section S3 and the results are summarized in Supporting Information Table S3. We used these experimentally determined data to parameterize a kinetic model, with which we analyzed the reaction fluxes through the various competing pathways. This model was first validated and found to adequately reproduce the experimentally observed dominance of trimer replicator in the absence of fueling, shown in Figure 2A (see Supporting Information Figure S20A for the modeled behavior). The model allowed concentrations and flow rates to be identified in which the oxidation and reduction fluxes go to a significant extent through the replicators. Furthermore, the model suggests that under the identified conditions, short-circuiting by direct reaction of perborate with TCEP occurred only to a minor extent (accounting for <0.1 % of the added oxidant and reductant). The flux through reduction and re-formation (by oxidation) of non-replicating small macrocycles (1%) was considerably smaller than the flux through the two replicator (together 99%). The fluxes through the different pathways obtained from the kinetic model are shown graphically by the thickness of the arrows in Figure 1B. Details of the model are provided in Supporting Information Section S4.

We then set up replicator competition experiments under conditions of concurrent perborate and TCEP fueled replicator formation and destruction. Specifically, we prepared an agitated mixture prepared from replicators $\mathbf{1}_3$ and $\mathbf{1}_6$ and non-assembled small macrocycles (predominantly $\mathbf{1}_3$ and $\mathbf{1}_4$) in a 15:30:55 ratio in terms of building block units (total concentration of 0.19 mM in **1**). TCEP and perborate redox reagents were infused simultaneously by separate syringe pumps. In order to compensate for the higher reactivity of TCEP the inflow of $NaBO_3$ was double that of TCEP for the first 4 hours of the experiment. Subsequently both reagents were flown in at the same rate in order to maintain a steady oxidation state. By flowing in 2.5 μL/hr of both reagent solutions (19 mM) into a 0.50 mL volume of replicator solution we achieved a nominal redox turnover time of 2 hours.

Operating the system in a fueled replication-destruction regime did indeed result in a steady state in which the slow and thermodynamically disfavored replicator $\mathbf{1}_6$ accounted for 60-70% of the building blocks in the mixture after 16 hours (Figure 4B and Supporting Information Figure S2). This steady state was maintained for 10 hours, corresponding to the total addition of 13 equivalents of $NaBO_3$ and 13 equivalents of TCEP. The fact that population of

replicator $\mathbf{1}_6$ occurs out of equilibrium and relies upon the supply of fuel was evident from the fact that, upon stopping the supply of fuel, the system reverted back to a replicator composition that is dominated by $\mathbf{1}_3$ (Figure 4B and Supporting Information Figure S2). Note that, when fueling was halted, initially only the $NaBO_3$ supply was stopped while addition of the TCEP solution was continued for at least 10 more hours (5 μL/hr flow rate) to prevent the excess amount of $NaBO_3$ that is present in the stationary state (and oxygen from the atmosphere) from completely oxidizing the sample and thereby freezing the disulfide exchange. Control experiments confirmed that the build-up of TCEP oxide as a waste product does not affect the relative thermodynamic stabilities of 3mer and 6mer replicators (see Supporting Information Figure S3). As shown above, performing the experiment of Figure 4B without fueling with oxidant and reductant resulted in the dominance of replicator $\mathbf{1}_3$ (Figure 3A).

The experimentally observed fueling-induced increase in the amount of hexamer replicator at the expense of trimer replicator (Figure 4B and Supporting Information Figure S2) was well reproduced in the kinetic model (see Supporting Information Figure S20B).

Achieving a state of dynamic kinetic stability (as opposed to thermodynamic equilibrium) in a system based on reversible disulfide chemistry is not trivial. The high rate of the disulfide exchange reaction offers a potentially fast competing pathway to equilibrium. Our kinetic analysis showed that disulfide exchange of non-assembled macrocycles in solution occurs on the second-minutes timescale ($k = 1.08 \pm 0.01 \times 10^4$ $M^{-1}s^{-1}$; Supporting Information Section S3.4). In the kinetic model the highest flux in the entire network is associated with the interconversion between non-assembled trimer and tetramer macrocycles (Supporting Information Table S7, reactions 5 and 6). However, as we showed previously, the rate of equilibration of disulfides slows down dramatically upon assembly of disulfides into stacks[33]. Indeed, upon stopping the supply of oxidant and reductant, the equilibration of replicator ring sizes occurs on the timescale of several days (Figure 4B). Thus, in the present system assembly is essential to allow a fueled out-of-equilibrium state to be maintained.

The molecularly more complex replicator is a better catalyst

These results show how chemical fueling enables the molecular complexification of the replicator, doubling its ring size. However, complexification is not an end by itself, but merely an enabler for the emergence of function. Among the most important functions in the transition from chemistry to biology is the ability to catalyze chemical reactions. In order to probe whether the complexification of the replicator structure enhances catalytic capability, we compared the abilities of both replicators to catalyze the retro-aldol reaction of substrate **2** (Figure 5A)[34], as a model chemical transformation. The data in Figure 5B shows that replicator $\mathbf{1}_6$ is indeed a more proficient catalyst than its molecularly less complex competitor $\mathbf{1}_3$ and also superior to the activity of non-assembled small rings (mixture dominated by $\mathbf{1}_3$ and $\mathbf{1}_4$) and building block **1**.

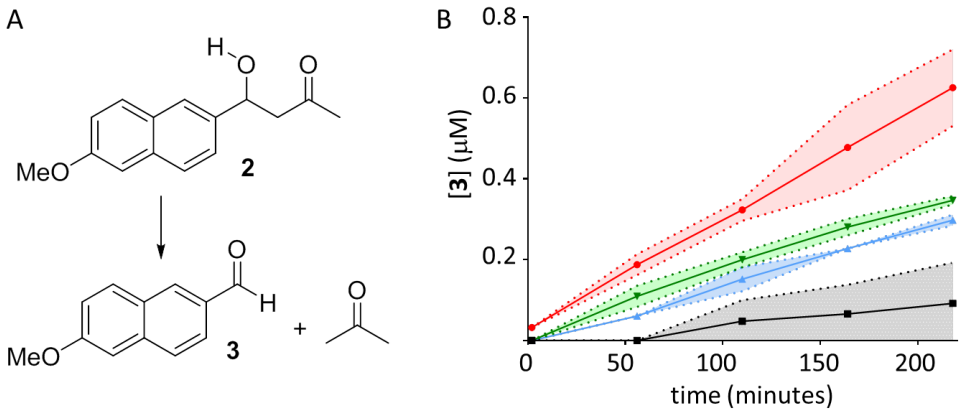

Fig. 5: The more complex replicator is a more proficient catalyst. (A) Retro-aldol reaction used as a model reaction to assess the catalytic proficiencies of the competing replicators. (B) Kinetic data, averaged over three repeats, comparing the production of retro-aldol product **3** catalyzed by replicator $\mathbf{1}_6$ (red circles) with the effects of replicator $\mathbf{1}_3$ (blue triangles), a mixture of non-assembled $\mathbf{1}_3$ and $\mathbf{1}_4$ (green triangles) and monomer **1** (black squares). The concentrations of the various species were 25 μM (in units of **1**) in borate buffer (50 mM, pH 8.12) containing 1.5 M guanidinium chloride and 0.20 mM substrate **2**. Shaded areas show the standard deviation and lines are drawn to guide the eye.

Conclusions

The above results represent the first experimental manifestation of molecular complexification in a replicator population that is not governed by thermodynamic stability or replication efficiency alone, but rather by, what Pross has termed, its dynamic kinetic stability[1,2].It extends beyond previous reports on dissipative system exhibiting physical autocatalysis (autopoietic micelle formation)[24] in that molecular information is copied through specific non-covalent interactions. Furthermore, unlike in the chemically fueled replication networks reported previously in which the one of the precursors of the replicator was continuously formed and broken down[25], in the present system the fuel acts directly on replicator destruction and re-formation.

Fueling enables populating molecularly more complex replicators that, in the absence of such energy supply, would not be able to compete with other, thermodynamically more stable or faster replicators. Such molecular complexification is made possible by conducting experiments in a regime where replication as well as replicator destruction take place simultaneously. Such regime results in a replicator distribution that is governed solely by balance between the rates of replication and destruction and requires an input of (chemical) energy to continuously cycle material between building blocks and replicators. Notably, in the present system the molecular complexification of the replicator is accompanied by improved function; the more complex replicator is a better catalyst for a model retro-aldol reaction than its less complex competing replicator. Establishing the principles that enable molecular complexification of a replicator clears an important hurdle in the process of the de-novo synthesis of life, facilitates functional improvement and, through that, may eventually enable open-ended evolution[8, 35]. These principles should be implementable in any system of replicators that feature, beside the

replication reaction, a path that deconstructs replicators back into building blocks. In addition this work is among the first examples of dissipative self-assembly in which more than a single bond is formed dissipatively[36]. It also shows that thiol-disulfide chemistry can be used to access out-of-equilibrium states, in which synthesis and degradation pathways through oxidation and reduction are faster than competing equilibration through thiol-mediated disulfide exchange. In the present system the ability to access a fueled out-of-equilibrium steady state relies critically on the inhibitory effect that the assembly of the disulfides into stacks has on disulfide exchange.

Methods

General procedures

All reagents, solvents and buffer salts were obtained from commercial suppliers and used without further purification, unless otherwise noted. Peptide building block **1** was synthesized by Cambridge Peptides Ltd (Birmingham, UK) from 3,5-bis(tritylthio)benzoic acid, which was prepared via a previously reported procedure[26]. Building block **4** and **5** (model compounds for kinetic studies, Supplementary Section S3) were synthesized by the same company. UPLC analyses were performed using a Waters Acquity UPLC H-class system with a reversed-phase UPLC column (Phenomenex Aeris Peptide, 2.1 × 150 mm; 1.7 μm). The column temperature was 35 °C and UV absorbance was monitored at 254 nm. Injection volumes were 2.5 μL (1:15 dilution in water with 0.6% TFA, where TFA was used to quench the disulfide exchange) and the eluent flow rate was 0.3 mL/min (see Supplementary Section S2 for the detailed method used). UPLC-MS analyses were performed on a Waters Xevo G2 UPLC/TOF. Electro-spray ionization was used to acquire positive-ion mass spectra. The capillary, sampling cone and extraction cone voltages were set at 2.5 kV, 30 kV and 4 V, respectively. Nitrogen was used as cone and desolvation gas with flow rates of 5 L/h and 500 L/h, respectively. The temperatures of source and desolvation were 150°C and 500°C, respectively. Transmission electron microscopy was performed on a Philips CM120 electron microscope operated at 120 kV. Images were recorded on a slow scan CCD camera (Gatan). Spectrophotometry measurements were performed on a Jasco V-650 spectrophotometer at 25 ºC and for fast kinetics a stopped-flow spectrometer with UV detector (SX20, from Applied Photophysics Limited, U.K.) was used. All concentrations involving $\mathbf{1_3}$, $\mathbf{1_4}$ and $\mathbf{1_6}$ are given with respect to building block **1**, unless stated otherwise. Representative UPLC

chromatograms and mass spectra of a mixture of macrocycles prepared from building block **1** are shown in Supplementary Figures S6-S10.

Replicator preparation (non-fueled)

Replicator experiments were conducted in UPLC vials (12 × 32 mm) with a Teflon-lined snap cap. Typically, building block **1** was dissolved to a concentration of 3.8 mM in borate buffer (50 mM in boron atoms, pH 8.2) for hexamer formation and in the same borate buffer containing 2.5 M guanidinium chloride for trimer formation. If needed, 1.0 M KOH solution was added to adjust the pH of the solution to 8.2. The volume of each sample was 1.0 mL. The replicators were the dominant products after 1 week of shaking the solutions at 1200 rpm (Eppendorf Thermomixer Comfort) in the presence of oxygen from the air.

Seeding experiments with $\mathbf{1}_3$ and $\mathbf{1}_6$

A solution of building block **1** (0.19 mM in borate buffer) was allowed to oxidize in air to give a mixture containing mostly unassembled 3mer (12%) and 4mer (11%) and monomer (60%). The resulting solution was split into three samples: to first two samples 3% and 6% (in monomer units) pre-formed $\mathbf{1}_3$ fibers were added, respectively. The last sample was not seeded. The concentration of guanidinium chloride was 1.5 M in all the samples, which were shaken at 1200 rpm. The sample compositions were monitored by UPLC over time.

For seeding experiments with $\mathbf{1}_6$ fibers, a solution of building block **1** (0.19 mM in borate buffer) was oxidized by sodium perborate to give a mixture containing 18% trimer, 14% tetramer and 43% monomer. The resulting solution was split into three samples which were seeded with no or 10 or 20% of pre-formed $\mathbf{1}_6$ fibers.

Thioflavine T (ThT) fluorescence

Solutions of $\mathbf{1}_3$ or $\mathbf{1}_6$ fibers (final concentration in building block **1** was 0.1 mM) were added to a ThT solution (final concentration 10 μM) in potassium borate buffer (50 mM, pH 8.2) in the presence (and for $\mathbf{1}_6$ fibers also in the absence) of 1.5M guanidinium chloride. Samples were incubated for 5 min and then transferred into a HELMA 10 × 2 mm quartz

cuvette. The fluorescence was measured on a JASCO FP6200 spectrophotometer (excitation at 440 nm, emission from 460 to 700 nm).

Comparison between the replication efficiencies of $\mathbf{1}_3$ and $\mathbf{1}_6$

First we introduced both replicators into a sample containing small non-assembled macrocycles ($\mathbf{1}_3$ and $\mathbf{1}_4$) and building block **1** in 1.5 M guanidinium chloride in the presence of oxygen from the atmosphere. Replicators $\mathbf{1}_3$ and $\mathbf{1}_6$ and non-assembled macrocycles were present in a 15:30:55 ratio in units of building block. The total building block concentration was 0.19 mM. The 0.50 mL sample was shaken at 1200 rpm in the presence of oxygen from the air. In this experiment both replicators compete for a common source of "food". The outcome of this competition is shown in Figure 3A.

In a separate set of experiments we added $\mathbf{1}_3$ and $\mathbf{1}_6$ separately to solutions containing building block **1** and non-assembled macrocycles ($\mathbf{1}_3$ and $\mathbf{1}_4$) in 1.5 M guanidinium chloride. To these samples we added perborate to oxidize the thiols to disulfides (Supporting Information, Figure S1). The reaction was performed in borate buffer with 1.5 M guanidinium chloride and $NaBO_3$ (5.0 μL, 38 mM) was added. The overall concentration in building block **1** was 0.19 mM.

Comparison between the thermodynamic stabilities of $\mathbf{1}_3$ and $\mathbf{1}_6$

The data in Figure 3B was obtained by mixing replicators $\mathbf{1}_3$ and $\mathbf{1}_6$ (approximately the same concentrations in units of **1**) and allowing this mixture to equilibrate while shaking at 1200 rpm in 1.5 M guanidinium chloride. To enable disulfide exchange 5 mol % of dithiol **1** was added and the overall concentration in building block **1** was 0.19 mM.

Comparison between the rate of reduction of $\mathbf{1}_3$ and $\mathbf{1}_6$

In order to assess the relative rates of reduction of replicators $\mathbf{1}_3$ and $\mathbf{1}_6$ we subjected a solution containing both replicators to TCEP as a reducing agent and monitored the relative extent to which the replicators diminished. Thus, samples with equimolar amounts of fibrous assemblies of replicators $\mathbf{1}_3$ and $\mathbf{1}_6$ (0.095 mM each with respect to building block **1**) were prepared by adding 12.5 μL $\mathbf{1}_3$ and $\mathbf{1}_6$ (3.8 mM in building block **1**) into borate buffer with 1.5

M guanidinium chloride to a final volume of 500 μL. The samples were then reduced 10%, 25% and 40% by adding corresponding amounts of a TCEP solution (19 mM). UPLC was used to analyze the composition of the samples directly after reduction (Figure 3C).

Replication-destruction experiments

A volume of 0.50 mL of a 1.5 M solution of guanidinium chloride in 50 mM borate buffer (pH 8.2) was placed in a glass UPLC vial (2 × 32 mm) to which replicators $\mathbf{1}_3$ and $\mathbf{1}_6$ were added to give a solution containing 50% (in units of building block) non-assembled $\mathbf{1}_3$ and $\mathbf{1}_4$, 5% **1** (allowing for disulfide exchange), 15% assembled replicator $\mathbf{1}_3$ and 30% replicator $\mathbf{1}_6$. The overall concentration in units of building block **1** was 0.19 mM. The sample was agitated by shaking on a thermomixer at 1200 rpm. Solutions of 19 mM sodium perborate and TCEP are dissolved in water, respectively (1.0 M solutions of HCl or NaOH were used to adjust the pH to 8.2), which were then transferred into two Hamilton syringes (100 μL). The syringes were placed in a syringe pump (Chemyx Fusion 200). To maintain a constant oxidation level, a higher initial flow of sodium perborate is needed due to the much lower reactivity of sodium perborate compared to TCEP. The flow rates of both redox reagents were kept at 2.5 μL/hr. The concentration of TCEP in the inflow syringe was 19 mM during the entire experiment, while a 38 mM solution of sodium perborate was flown in for the first 4 hours. Subsequently the perborate solution was replaced with a 19 mM one for the remainder of the experiment. The experiment was performed in an open vial and the flow rate was tuned to compensate for the volume loss due to evaporation, keeping the total volume approximately constant. Given that the concentration of building block is 0.19 mM and concentration of redox reagents is 19 mM (overall sample volume is 500 μL) and the flow rate is 2.5 μL/hr, the redox turnover time of the sample is 2 hours. The flow of $NaBO_3$ was stopped after 27 hours. Due to lower reactivity of sodium perborate compared to TCEP, perborate accumulates at the steady state. In order to neutralize the excess perborate, 3.8 mM TCEP was added for 10 hours at a flow rate of 5 μL/hr after the perborate flow was stopped. The concentration of dithiol **1** remains approximately constant during the entire experiment. The composition of the libraries was monitored by UPLC. A control experiment was also performed starting with the same sample composition but without flowing in any redox reagents (Figure 3A).

Effect of TCEP oxide as a waste product

TCEP oxide was prepared through the reaction between TCEP and $NaBO_3$. The complete conversion from TCEP to TCEP oxide was confirmed by Ellman's assay[37]. Samples containing equal amount of assembled $\mathbf{1}_6$ and assembled $\mathbf{1}_3$ (0.095 mM in building block **1** each), and 5% dithiol **1** were prepared in borate buffer (pH 8.2) with 1.5 guanidinium chloride and split into two parts: to the first one TCEP oxide (4.56 mM) was added, to an amount that is equivalent to the amount that had accumulated in the replication-destruction setup after 48 h; the second one served as a control, as no TCEP oxide was added (Supporting Information Figure S3). The experiments were performed under shaking at 1200 rpm.

Catalysis of the retro-aldol reaction by trimer and hexamer replicators

A solution containing 1.5 M guanidinium chloride and either 25 µM (in units of building block **1**) assembled trimers, hexamers, monomers or oxidized monomers was prepared in 980 µL borate buffer (50 mM, pH 8.12) using a UPLC vial (12 x 32 mm). Then, 20 µL of a 10 mM stock solution of methodol in acetonitrile was added to the vial, after which the reaction mixture was monitored through periodic UPLC analysis at 25°C (10 µL injection of the mixture, 54 minute intervals). The concentration of 6-methoxy-2-naphthaldehyde was quantified by comparison to a calibration curve, that was obtained by injecting known quantities of 6-methoxy-2-naphthaldehyde in the reaction buffer (λ max = 313 nm). All reactions were monitored in triplicate.

Data availability: The raw datasets generated during and/or analyzed during the current study are available from the corresponding author on reasonable request.

Code availability: The computer code used in the flux analysis is available from the corresponding author on reasonable request.

References

1. Pross, A. Towards a general theory of evolution: extending Darwinian theory to inanimate matter. *J. Syst. Chem.* **2**, 1 (2011).
2. Pross, A. *What is life? How chemistry becomes biology*. (Oxford University Press, Oxford, 2012).
3. Ruiz-Mirazo, K., Briones, C., De la Escosura, A. Prebiotic systems chemistry: New perspectives for the origins of life. *Chem. Rev.* **114**, 285-366 (2014).
4. Szostak, J.W. The narrow road to the deep past: In search of the chemistry of the origin of life. *Angew. Chem. Int. Ed.* **56**, 11037-11043 (2017).
5. Patzke, V., von Kiedrowski, G. Self replicating systems. *Arkivoc* **v**, 293-310 (2007).
6. Clixby, G., Twyman, L. Self-replicating systems. *Org. Biomol. Chem.* **14**, 4170-4184 (2016).
7. Bissette, A.J., Fletcher, S.P. Mechanisms of autocatalysis. *Angew. Chem. Int. Ed.* **52**, 12800-12826 (2013).
8. Duim, H., Otto, S. Towards open-ended evolution in self-replicating molecular systems. *Beilstein J. Org. Chem.* **13**, 1189–1203 (2017).
9. Kosikova, T., Philp, D. Exploring the emergence of complexity using synthetic replicators. *Chem. Soc. Rev.* **46**, 7274-7305 (2017).
10. Diaz Arenas, C., Lehman, N. Quasispecies-like behavior observed in catalytic RNA populations evolving in a test tube. *BMC Evol. Biol.* **10**, 80 (2010).
11. Robertson, M.P., Joyce,G.F. Highly efficient self-replicating RNA enzymes. *Chem. Biol.* **21**, 238-245 (2014).
12. Mills, D.R., Peterson, R.L., Spiegelman, S. An extracellular Darwinian experiment with a self-duplicating nucleic acid molecule. *Proc. Natl. Acad. Sci. U. S. A.* **58**, 217-224 (1967).

13. Kreysing, M., Keil, L., Lanzmich, S. & Braun, D. Heat flux across an open pore enables the continuous replication and selection of oligonucleotides towards increasing length. *Nat. Chem.* **7**, 203-208 (2015).

14. Bansho, Y., Furubayashi, T., Ichihashi, N. & Yomo, T. Host-parasite oscillation dynamics and evolution in a compartmentalized RNA replication system. *Proc. Natl. Acad. Sci. U.S.A.* **113**, 4045-4050 (2016).

15. Matsumura, S. *et al.* Transient compartmentalization of RNA replicators prevents extinction due to parasites. *Science* **354**, 1293-1296 (2016)

16. Boekhoven, J. *et al.*, Dissipative self-assembly of a molecular gelator by using a chemical fuel. *Angew. Chem. Int. Ed.* **49**, 4825-4828 (2010).

17. Wilson, M.R. *et al.*, An autonomous chemically fuelled small-molecule motor. *Nature* **534**, 235-240 (2016).

18. Maiti, S., Fortunati, I., Ferrante, C., Scrimin, P., Prins, L.J. Dissipative self-assembly of vesicular nanoreactors. *Nat. Chem.* **8**, 725-731 (2016).

19. van Esch, J.H., Klajn, R., Otto, S. Chemical systems out of equilibrium. *Chem. Soc. Rev.* **46**, 5474-5475 (2017).

20. Erbas-Cakmak, S. *et al.*, Rotary and linear molecular motors driven by pulses of a chemical fuel. *Science* **358**, 340-343 (2017).

21. Sorrenti, A., Leira-Iglesias, J., Sato, A., Hermans, T.M. Non-equilibrium steady states in supramolecular polymerization. *Nat. Commun.* **8**, 15899 (2017).

22. Ragazzon, G., Prins, L.J. Energy consumption in chemical fuel-driven self-assembly. *Nature Nanotechnology* **13**, 882-889 (2018).

23. Astumian, R.D. Stochastic pumping of non-equilibrium steady-states: how molecules adapt to a fluctuating environment. *Chem. Commun.* **54**, 427-444 (2018).

24. Morrow, S.M., Colomer, I., Fletcher, S.P. A chemically fuelled self-replicator. *Nat. Commun.* **10**, 1011 (2019).

25. Maity, I., Wagner, N., Mukherjee, R. et al. A chemically fueled non-enzymatic bistable network. *Nat. Commun.* **10**, 4636 (2019).

26. Carnall, J.M.A. *et al.*, Mechanosensitive self-replication driven by self-organization. *Science* **327**, 1502-1506 (2010).

27. Malakoutikhah, M. *et al.*, Uncovering the selection criteria for the emergence of multi-building-block replicators from dynamic combinatorial libraries. *J. Am. Chem. Soc.* **135**, 18406-18417 (2013).

28. Colomb-Delsuc, M., Mattia, E., Sadownik, J.W., Otto, S. Exponential self-replication enabled through a fibre elongation/breakage mechanism. *Nat. Commun.* **6**, 7427 (2015).

29. Sadownik, J.W., Mattia, E., Nowak, P., Otto, S. Diversification of self-replicating molecules. *Nat. Chem.* **8**, 264-269 (2016).

30. Otto, S., Furlan, R.L.E., Sanders, J.K.M. Dynamic combinatorial libraries of macrocyclic disulfides in water. *J. Am. Chem. Soc.* **122**, 12063-12064 (2000).

31. Bertz, S. H., The first index of molecular complexity. *J. Am. Chem. Soc.* **103**, 3599-3601 (1981).

32. Böttcher, T., An additive definition of molecular complexity. *J. Chem. Inf. Model.* **56**, 462-470 (2016).

33. Mattia, E., Pal, A., Leonetti, G. & Otto, S. Mechanism of Building Block Exchange in Stacks of Self-Replicating Macrocycles. *Synlett* **28**, 103-107 (2017).

34. Ottelé, J. O., Hussain, A. S., Mayer, C., Otto, S. Chance emergence of catalytic activity and promiscuity in a self-replicator. *ChemRxiv* doi: 10.26434/chemrxiv.10002032 (2019).

35. Ruiz-Mirazo, K., Pereto, J., Moreno, A. Defining life or bringing biology to life. *Orig. Life Evol. Biosph.* **40**, 203-213 (2010).

36. Hossain, M. M.; Atkinson, J.; Hartley, S. Chemically Fueled Assembly of Macrocycles Comprising Multiple Transient Bonds. *ChemRxiv*. doi: 10.26434/chemrxiv.11426007.v1 (2019).

37. Han, J.C., Han, G.Y. A procedure for quantitative-determination of tris(2-carboxyethyl)phosphine, an odorless reducing agent more stable and effective than dithiothreitol. *Anal. Biochem.* **220**, 5-10 (1994).

Acknowledgements: We gratefully acknowledge funding from the China Scholarship Council to SY, the NWA StartImpuls to O.M., the Netherlands Organisation for Scientific Research (Vici grant 724.012.002), the ERC (AdG 741774) and the Dutch Ministry of Education, Culture and Science (Gravitation program 024.001.035). We thank Albertas Janulevicius for help with debugging the code for the kinetic model.

Author contributions: S.O. supervised the overall project. S.Y. conceived and designed the study, performed the experiments and analyzed the data. G.S, A.S.H, J.O, K.L. and A.S. performed the experiments and analyzed the data. E.M. and O.M. performed computational experiments. S.Y, G.S, O.M. and S.O. co-wrote the paper. All authors discussed the results and commented on the manuscript.

Competing interests: the authors declare no competing interests.

Additional information

Supplementary information is available for this paper and can be found below.

Correspondence and requests for materials should be addressed to S.O..

SUPPORTING INFORMATION

Chemical Fueling Enables Molecular Complexification of Assembly-Driven Self-Replicators

Shuo Yang, Gael Schaeffer, Elio Mattia, Omer Markovitch, Kai Liu, Andreas S. Hussain, Jim Ottelé, Ankush Sood, Sijbren Otto*

University of Groningen, Center for Systems Chemistry, Stratingh Institute for Chemistry, Nijenborgh 4, 9747 AG Groningen, The Netherlands.

*E-mail corresponding author: s.otto@rug.nl

Content

S1. Supplementary Figures

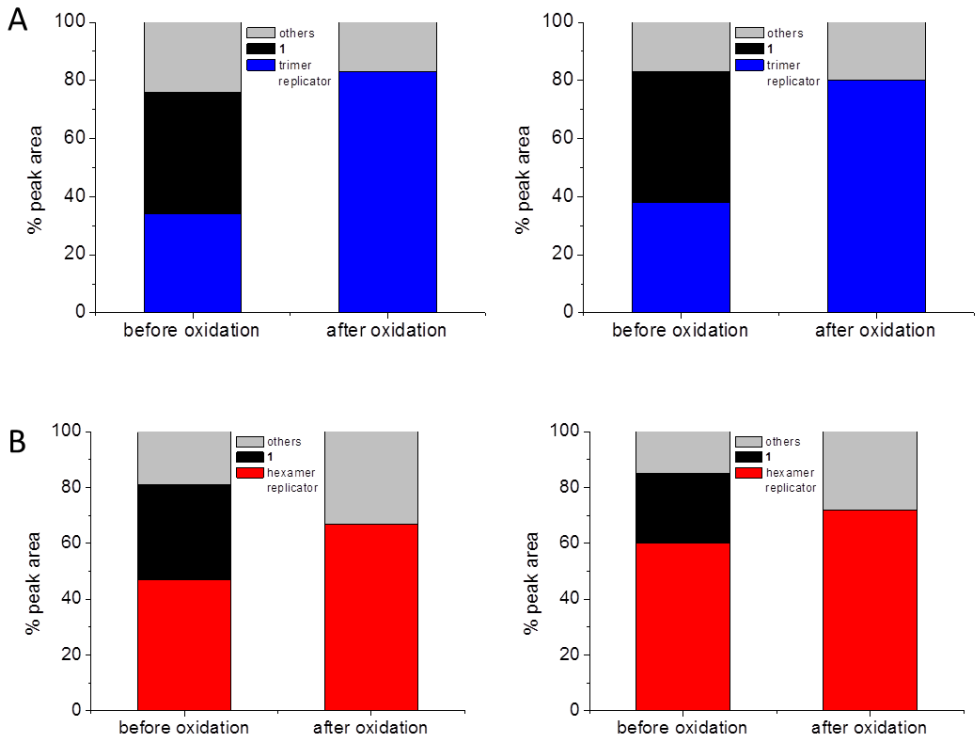

Figure S1. Self-Replication upon oxidation by $NaBO_3$. (A) Duplicates of the growth of replicator $\mathbf{1}_3$ upon oxidation of a mixture containing pre-formed replicator $\mathbf{1}_3$ (blue), monomer **1** (black) and non-assembled small macrocycles (mostly trimer and tetramer; grey). The reaction was performed in borate buffer with 1.5 M guanidinium chloride and $NaBO_3$ (5.0 μL, 38 mM) was added (overall concentration in building block **1** was 0.19 mM). For the sample containing $\mathbf{1}_3$ replicator almost all **1** was converted to $\mathbf{1}_3$. We suspect this to be assembled $\mathbf{1}_3$ replicator, since the amount of $\mathbf{1}_4$ (that is in fast equilibrium with non-assembled $\mathbf{1}_3$) remains almost constant. (B) Duplicates of the growth of replicator $\mathbf{1}_6$ upon oxidation of a mixture containing pre-formed replicator $\mathbf{1}_6$ (red), monomer **1** (black) and non-assembled small macrocycles (mostly trimer and tetramer; grey). The reaction was performed in borate buffer (pH 8.2) with 1.5 M guanidinium chloride and $NaBO_3$ (5.0 μL, 38 mM) was added (the overall concentration in building block **1** is 0.19 mM). The reactions were monitored by UPLC. In contrast to panel A, for the sample containing $\mathbf{1}_6$ the conversion of **1** to replicator was only partial and accompanied by the formation of a significant fraction of non-assembling small macrocycles (grey).

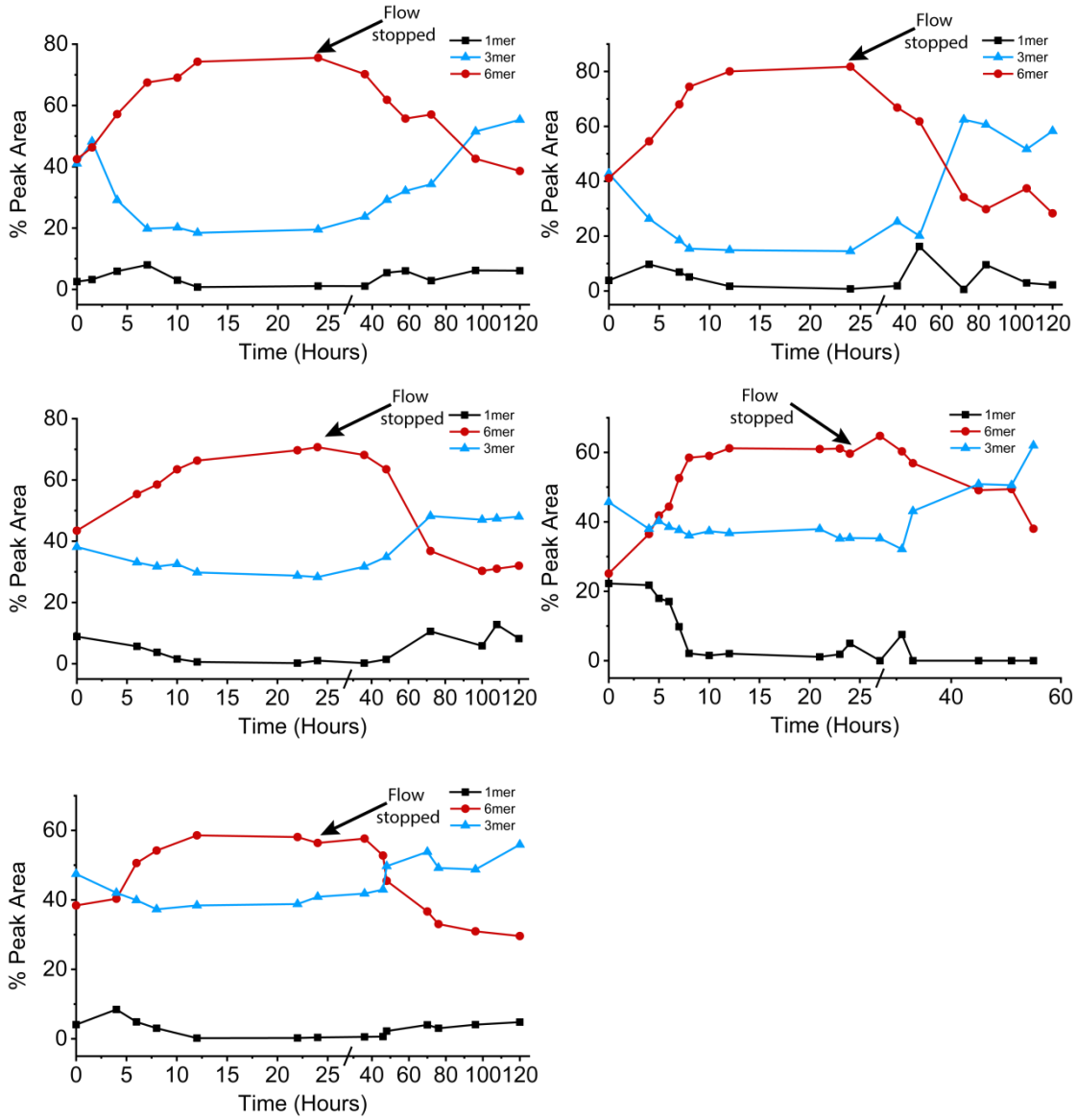

Figure S2. Five repeats of the experiment in Figure 4B. Evolution of the product distribution with time upon continuous and simultaneous addition of TCEP and $NaBO_3$ solutions to a mixture (0.50 mL) initially containing replicators $\mathbf{1}_3$ and $\mathbf{1}_6$ and non-assembled **1**, $\mathbf{1}_3$ and $\mathbf{1}_4$ (overall 0.16 mM in **1**) in 50 mM borate buffer (pH 8.2) containing 1.5 M guanidinium chloride. At t = 0-24h $NaBO_3$ (26.5mM) was flow in at 2.5 µL/h, and TCEP (19 mM) flown in at 2.5 µL/h. At t = 25-50h TCEP (3.8 mM) flow in at 2.5 µL/h. Lines are drawn to guide the eye.

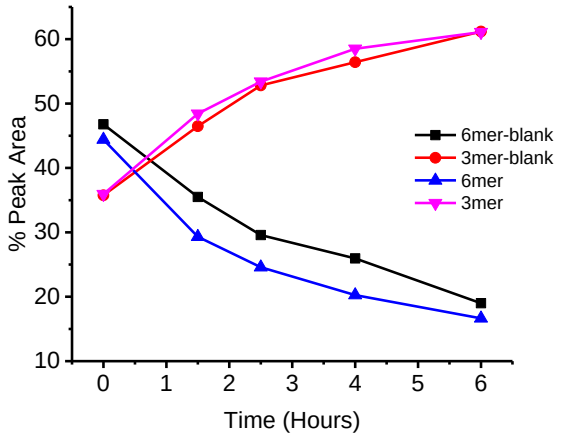

Figure S3. Effect of TCEP oxide waste. Change in product distribution with time of a mixture of replicators $\mathbf{1}_6$ to $\mathbf{1}_3$ (0.095 mM in building block **1** each) and 5% dithiol **1** in 1.5 M guanidinium chloride in the absence (blank) and presence of TCEP oxide (4.56 mM, equivalent to the amount that had accumulated in the replication-destruction setup after 48 h of operation). Comparison of the behavior of both samples reveals that TCEP oxide has no significant effect on the relative stabilities and rates of interconversion of replicators $\mathbf{1}_6$ and $\mathbf{1}_3$. Lines are drawn to guide the eye.

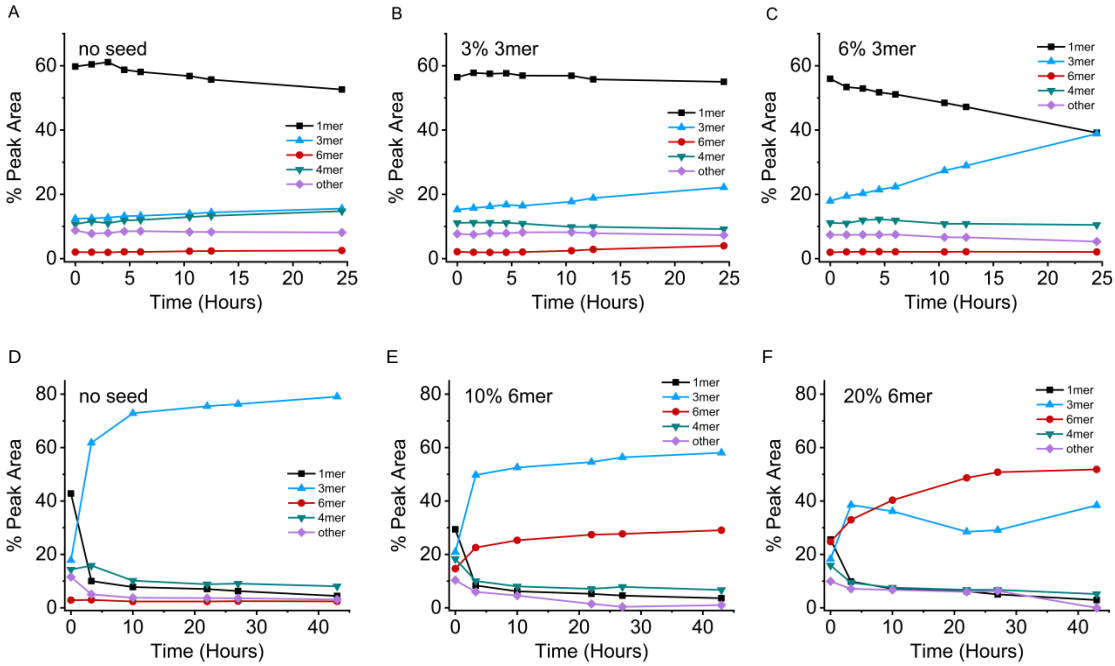

Figure S4. Complete data for the experiments shown in Figure 2C and D. (A-C): Change in product distribution with time of a pre-oxidized (by oxygen in the air) sample made from **1** (0.19 mM) in borate buffer pH 8.2 in the presence of 1.5 M guanidinium chloride in the absence (A) and presence of 3% (B) and 6% (C) seeds of $\mathbf{1}_3$ replicator. (D-E): Change in product distribution with time of a pre-oxidized (by sodium perborate) sample made from **1** (0.19 mM) in borate buffer pH 8.2 in the presence of 1.5 M guanidinium chloride (A) in the absence and presence of 10% (B) and 20% (C) seeds of $\mathbf{1}_6$ replicator. Seeding % are expressed in units of **1** relative to the total number of units of **1**. Lines are drawn to guide the eye.

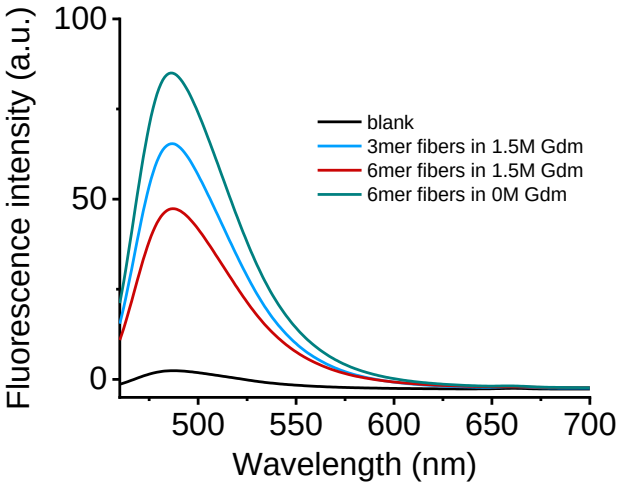

Figure S5. Extent of β-sheet formation of replicators in different media. Fluorescence emission spectra of solutions of thioflavin T (final concentration 10 μM) in the presence of assembled $\mathbf{1}_3$ in 1.5 M guanidinium chloride (blue line) and $\mathbf{1}_6$ in1.5 M guanidinium chloride (red line) and 0 M guanidinium chloride (green line). The final concentrations of $\mathbf{1}_3$ and $\mathbf{1}_6$ are all 0.1 mM (in units of **1**). No fibers were added in the blank sample (black line).

S2. UPLC-MS analysis of the reaction mixtures

Table S1. UPLC method for the analysis of the reaction mixtures

Time (min)	% water + 0.1% TFA	% MeCN + 0.1% TFA
0	90	10
1	90	10
1.3	75	25
3	72	28
11	60	40
11.5	5	95
12	5	95
12.5	90	10
17	90	10

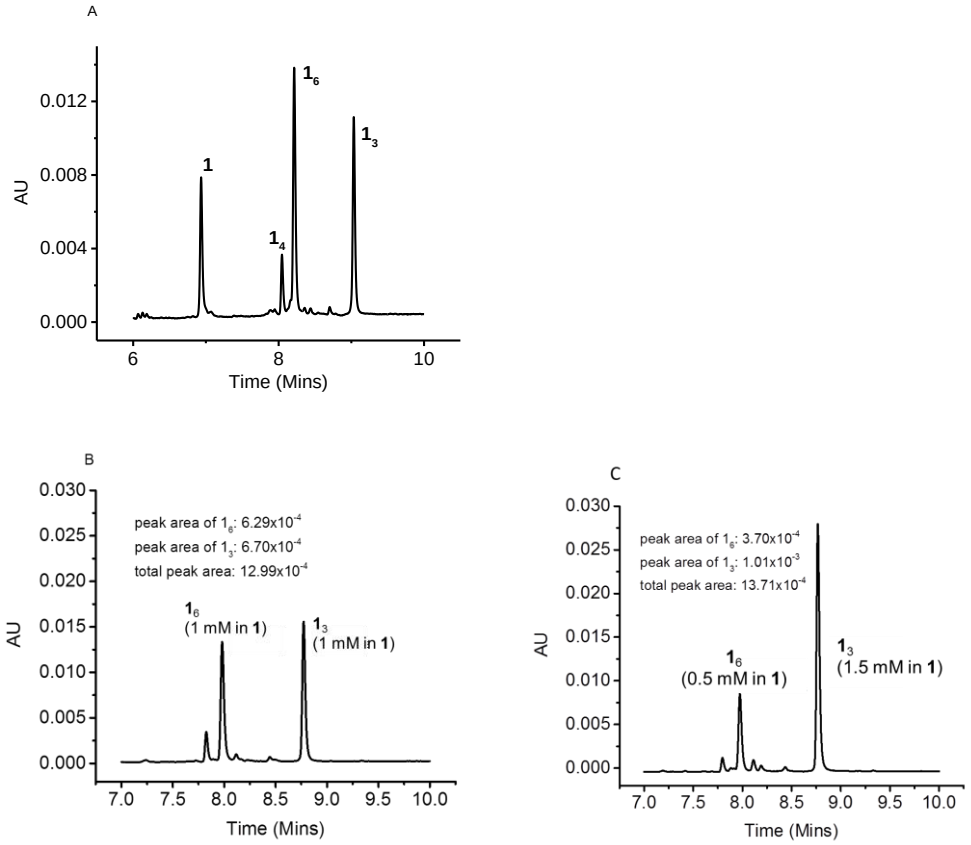

Figure S6. (A) Representative UPLC chromatogram of a mixture of macrocycles prepared from building block **1**. (B) Representative UPLC chromatograms of mixtures with different amounts of $\mathbf{1}_3$ and $\mathbf{1}_6$ showing a comparable total peak area, indicating that the molar absorptivity of the building block is independent of the macrocycle in which it resides. Thus, relative peak areas can be used to quantify the amount of these replicators.

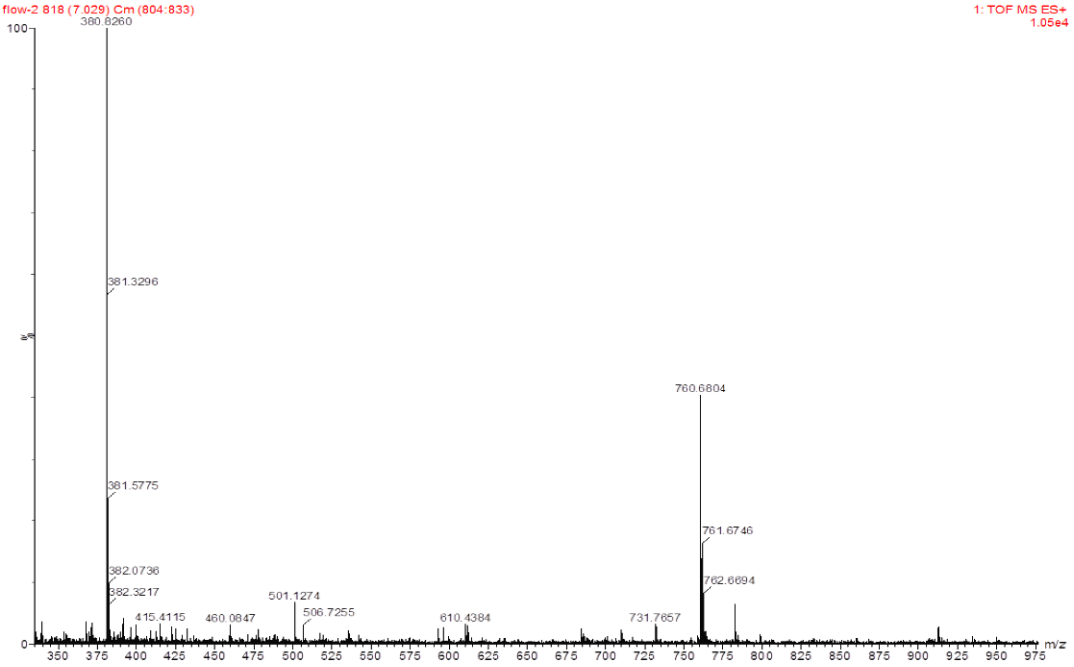

Figure S7. Mass spectrum of monomer **1** from the LC-MS analysis of a DCL made from **1**. M/z calculated: 760.35 $[M+H]^{1+}$, 380.68 $[M+2H]^{2+}$; m/z observed: 760.68 $[M+H]^{1+}$, 380.82 $[M+2H]^{2+}$.

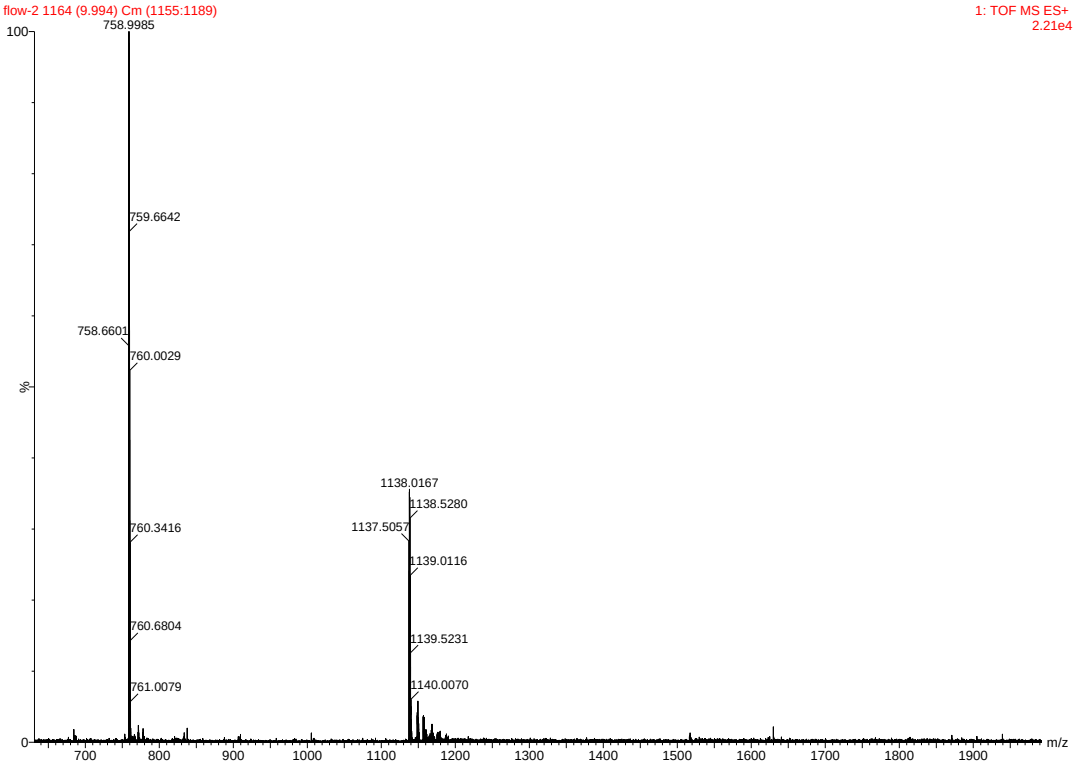

Figure S8. Mass spectrum of $\mathbf{1}_3$ from the LC-MS analysis of a DCL made from **1**. M/z calculated: 1137.50 $[M+2H]^{2+}$, 759.01 $[M+3H]^{3+}$; m/z observed: 1137.50 $[M+2H]^{2+}$, 758.66 $[M+3H]^{3+}$.

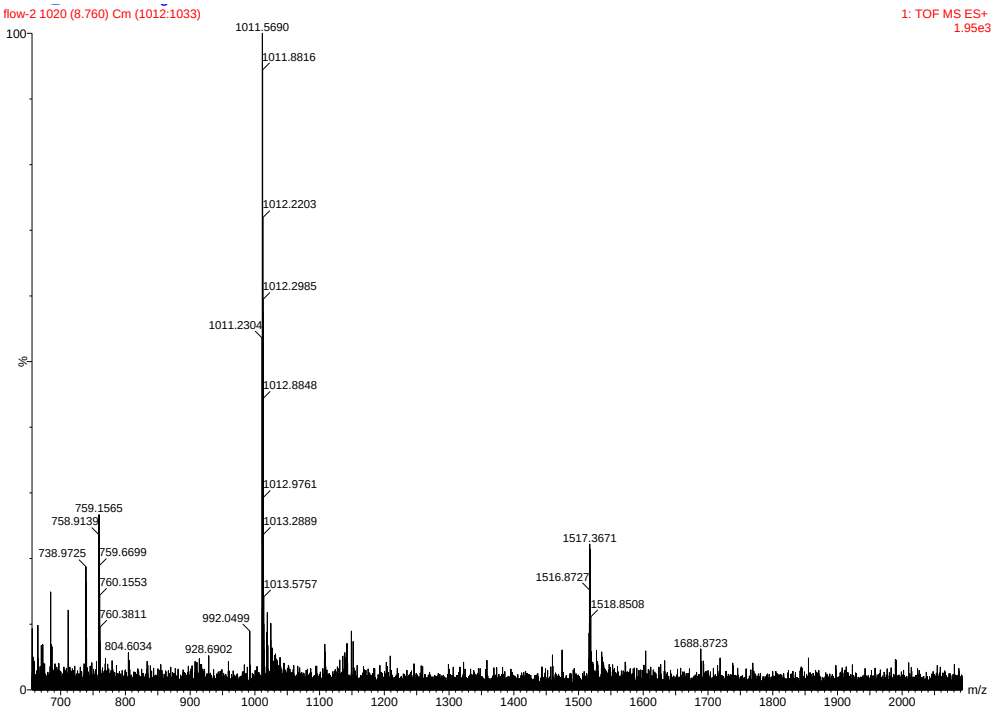

Figure S9. Mass spectrum of $\mathbf{1}_4$ from the LC-MS analysis of a DCL made from **1**. M/z calculated: 1516.67 $[(M+2)+2H]^{2+}$, 1011.45 $[(M+2)+3H]^{3+}$, 758.59 $[(M+1)+4H]^{4+}$; m/z observed: 1516.87 $[(M+2)+2H]^{2+}$, 1011.23 $[(M+2)+3H]^{3+}$, 758.91 $[(M+1)+4H]^{4+}$.

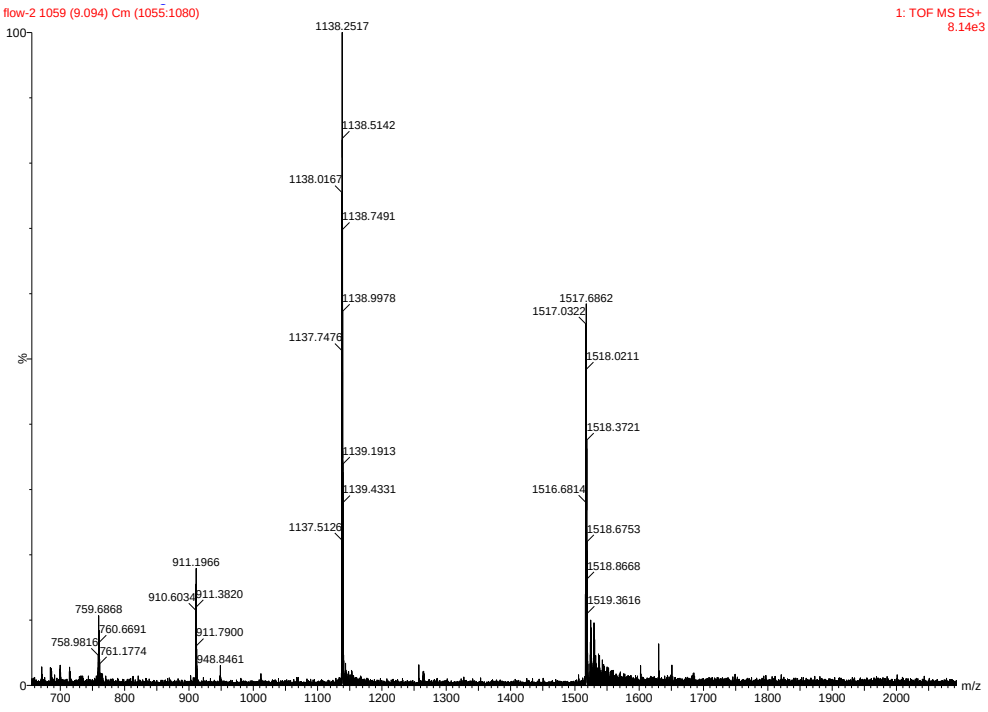

Figure S10.. Mass spectrum of $\mathbf{1}_6$ from the LC-MS analysis of a DCL made from **1**. M/z calculated: 1516.67 $[(M+3)+3H]^{3+}$, 1137.75 $[(M+3)+4H]^{4+}$, 910.80 $[(M+5)+5H]^{5+}$, 759.00 $[(M+4)+6H]^{6+}$;m/z observed: 1516.68 $[(M+3)+3H]^{3+}$, 1137.51 $[(M+3)+4H]^{4+}$, 910.60 $[(M+5)+5H]^{5+}$, 758.98 $[(M+4)+6H]^{6+}$

.

S3. Kinetics of individual reactions

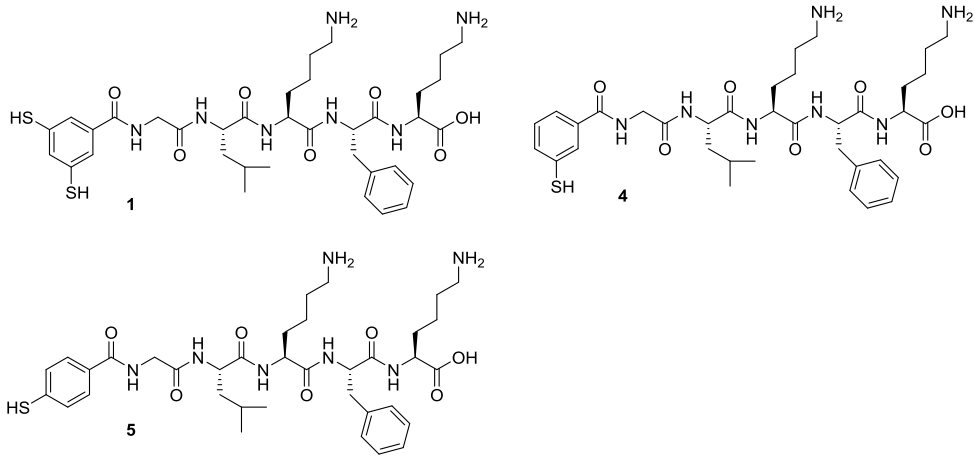

S3.1 Sodium perborate mediated thiol oxidation

To measure the rate of thiol oxidation by sodium perborate, monothiol building block **4** was used. Both building block **4** and $NaBO_3$ were dissolved in borate buffer (50 mM, pH 8.2) at a concentration of 1.0 mM as stock solutions which were diluted further for kinetic measurement. The concentration of thiol **4** was monitored at 274 nm (wavelength where the thiol group absorbs, but where the absorbance of disulfide $\mathbf{4}_2$ is relatively low). The overall absorbance A of the sample at this wavelength can be expressed as:

$$A = A_m + A_d = \varepsilon_m C_m l + \varepsilon_d C_d l$$

Where subscript m stands for monomer **4**, d for disulfide dimer $\mathbf{4}_2$; ε is the molar absorption coefficient, C represents the concentration and l represents the length of the light path through the sample.

The overall concentration of building block C is known, where $C = C_m + 2C_d$, and l is 1.00 cm, so the above equation can be rewritten as:

$$A = (\varepsilon_m - 0.5\varepsilon_d)C_m + 0.5\varepsilon_d C$$

Thus, the absorbance of the sample is proportional to the concentration of the monomer. The coefficients ε_m and ε_d were determined experimentally (linear fit using

absorbance data at five different concentrations) yielding ε_m = 8848 $M^{-1}cm^1$ (R^2 = 0.9999) and ε_d = 4953 $M^{-1}cm^1$ (R^2 = 0.9966).

Firstly, through fixing the concentration of one of the reactants and varying the concentration of the other, then plotting the varied concentrations versus the corresponding initial rates on a log-log plot, the orders in the reactants were obtained. Five concentrations were used and for each concentration the experiment was repeated three times. Each experiment was monitored for 1 hour (Figure S11).

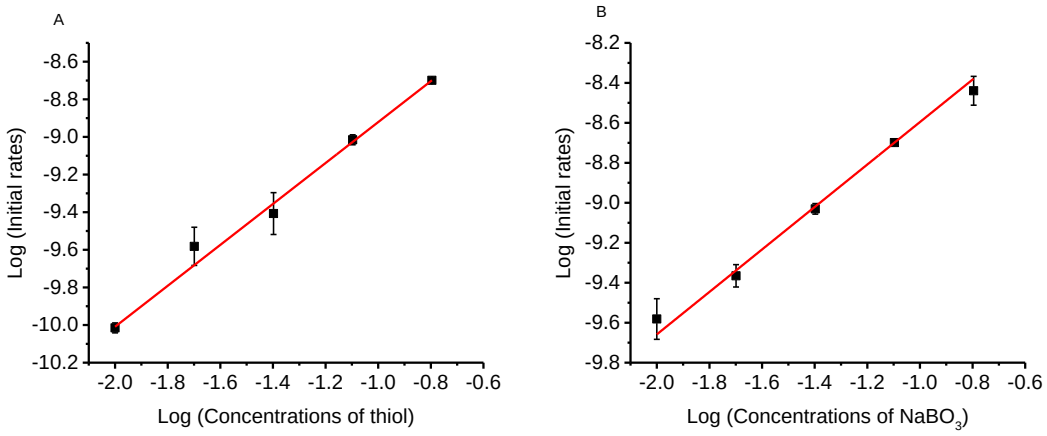

Figure S11. Determination of orders in reactants in the oxidation reaction. Log-log plot of concentrations versus initial rates. (A) The concentration of $NaBO_3$ was fixed at 0.020 mM and the concentrations of **4** were 0.0050, 0.010, 0.020, 0.040, 0.080 mM. (B) The concentration of **4** was fixed at 0.020 mM and the concentrations of $NaBO_3$ were 0.010, 0.020, 0.040, 0.080 and 0.16 mM. The order of thiol and sodium perborate are both taken as 1 (measured order in thiol is 1.06; R^2 = 0.9885; measured order of sodium perborate is 0.98; R^2 = 0.9552). Lines represent fits of the data.

Then the rate constant for the thiol oxidation reaction was determined based on a second-order rate equation. The concentrations of reactants were both 0.020 mM. The kinetics were followed by UV spectroscopy in borate buffer (pH 8.2) at 25 °C. The reactions were monitored for 30 mins (sampling time every 8 seconds) and repeated three times (Figure S12).

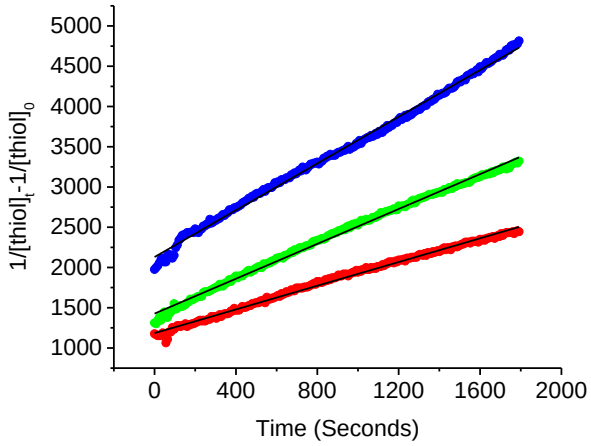

Figure S12. Kinetic data for the reaction of thiol 4 with $NaBO_3$, Three repeats of the same experiment are indicated in different colors and the curves fitted to the individual datasets are shown in black. The terms $[thiol]_t$ and $[thiol]_0$ refer to the concentration of thiol **4** at times t and t=0, respectively. The rate constant for the oxidation reaction was found to be 1.09 (±0.35) $M^{-1}s^{-1}$.

S3.2 TCEP mediated disulfide reduction

The process for measuring the order in reactants and rate constant for the reduction of dimer $\mathbf{4}_2$ by TCEP was similar to that reported for borate mediated thiol oxidation. However, a stopped-flow spectrometer with UV detector was used due to the fast kinetics. Firstly solutions containing disulfide and TCEP (0.5 mL each) were loaded into two syringes, respectively, which were then forced into a mixing chamber for few milliseconds. The chamber then acted as an observation cell where the UV absorbance at 274 nm was recorded.

Through fixing the concentration of one of the reactants and varying the concentration of the other, then plotting the varied concentrations versus the corresponding initial rates on a log-log plot, the orders in the reactants were obtained. The determination of the order in each reactant was based on five concentrations and each experiment at each concentration was repeated three times. Each experiment was monitored for 0.5 seconds (Figure S13).

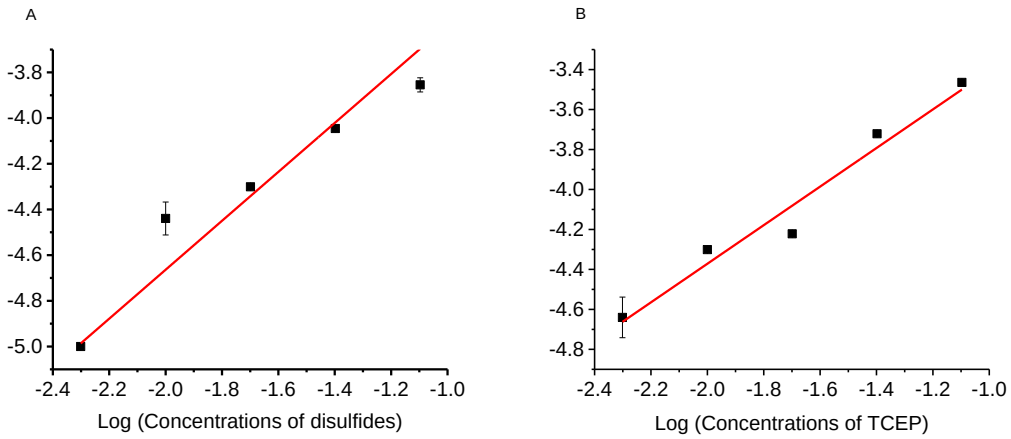

Figure S13. Determination of orders in reactants in the reduction reaction. Log-log plot of concentrations versus initial rates. (A) The concentration of TCEP was fixed at 0.020 mM and the concentrations of $\mathbf{4_2}$ were 0.005, 0.01, 0.02, 0.04, 0.08 mM. (B) The concentration of $\mathbf{4_2}$ was fixed at 0.020 mM and the concentrations of TCEP were 0.005, 0.01, 0.02, 0.04 and 0.08 mM. The order of the reaction in disulfide and TCEP are both taken as 1 (the measured order in disulfide is 1.071; R^2 = 0.9929; the measured order in TCEP is 0.9652; R^2 = 0.8071). Lines represent fits of the data.

The concentrations of reactants used for measuring the rate constant were 0.020 mM each. The kinetics were followed using a stopped-flow spectrometer in borate buffer (pH 8.2) at 25 °C. The reaction were monitored for 0.1 seconds (sampling every 0.0002 seconds) and were repeated three times (Figure S14).

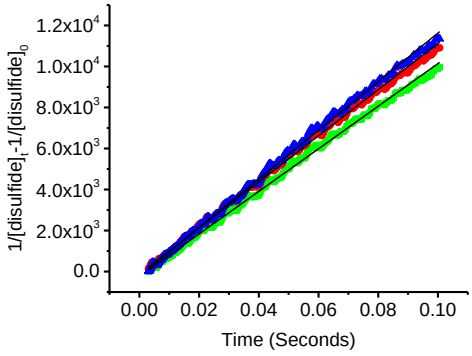

Figure S14. Kinetic data for the reaction of disulfide $\mathbf{4_2}$ with TCEP. Three repeats of the same experiment are indicated in different colors and the curves fitted to the individual datasets are shown in black. The terms $[disulfide]_t$ and $[disulfide]_0$ refer to the concentration of disulfide $\mathbf{4_2}$ at times t and t=0,

respectively. The rate constant was obtained through fitting the data to a second-order rate equation, resulting in a value of 1.11 (± 0.8) × 10^5 $M^{-1}s^{-1}$.

S3.3. Quenching reaction between TCEP and $NaBO_3$

The rate constant of the reaction between TCEP and $NaBO_3$ was determined by mixing equimolar amounts of TCEP and $NaBO_3$ and letting the solution incubate for various amounts of time. Given that TCEP reduction is several orders of magnitude faster than oxidation by $NaBO_3$ (see above), the incubated mixture of TCEP/$NaBO_3$ was added to $\mathbf{1}_3$. This solution was then quickly analyzed by UPLC and the amount of monomer present in the UPLC trace was estimated as a function of the incubation time. Upon addition of the TCEP/$NaBO_3$ mixture to $\mathbf{1}_3$ fibers we assume that during the first minutes only reduction of the fibers is observed and that the amount of oxidation of the monomer can be neglected (the large difference between the rate constants for oxidation and reduction determined above supports this assumption).

A 5.00 mM solution of TCEP was prepared by dissolving 1.83 mg of TCEP in 1.275 mL double distilled water. Similarly, a 5.00 mM $NaBO_3$ solution was prepared by dissolving 2.19 mg $NaBO_3$ in 2.80 mL water and sonicating this mixture for 5 min. to ensure all the material is dissolved. An aliquot of 25 μL of the TCEP solution was added to 25 μL of the $NaBO_3$ solution and these mixtures were incubated for various amounts of time (0, 30, 60, 120 and 180 s). After incubation, 9.75 μL of the solution was added to 86 μL of assembled $\mathbf{1}_3$ at 1.06 mM in 1.68 M guanidinium chloride (therefore, after addition [$\mathbf{1}_3$] = 0.95 mM and [guanidinium chloride] = 1.5 M). The solution was shaken for 5 seconds and 5 μL were sampled for immediate UPLC analysis (Supplementary Table S2).

Table S2: **Kinetic data of the quenching reaction of $NaBO_3$ with TCEP.** Fraction of monomer (from UPLC integration) and monomer concentration after mixing incubated (TCEP + $NaBO_3$) with assembled $\mathbf{1}_3$ and incubation for various durations.

Incubation time (sec)	0	30	60	120	180
% **1** (UPLC)	42.2	42.1	41.8	41.4	40.8
[**1**] = [TCEP]	0.000401	0.0004	0.000397	0.000393	0.000388

The amount of monomer observed by UPLC should equal the amount of TCEP left to react after incubation with $NaBO_3$. From previous kinetic analyses, we assumed that for the reaction between TCEP and $NaBO_3$, the order in both reagents is 1, leading to a total reaction order of 2. In order to determine the second-order rate constant for the reaction between TCEP and $NaBO_3$ we plotted $1/[C]-1/[C_0]$ (where [C] is the TCEP concentration) versus incubation time (Figure S15).

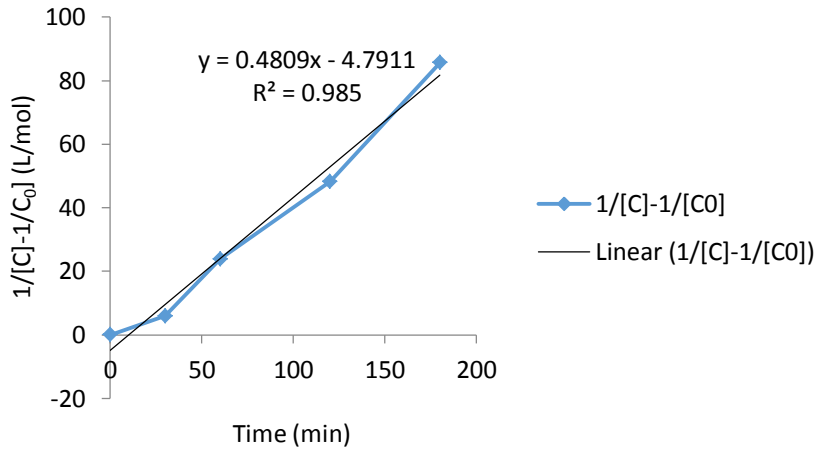

Figure S15. Kinetic analysis of the quenching reaction of $NaBO_3$ with TCEP. The slope of this curve gives an estimate of the rate constant for the quenching reaction of 0.5 (± 0.2) $M^{-1} \cdot s^{-1}$.

S3.4 Disulfide exchange

To measure the rate of thiol-disulfide exchange model compounds **4** and $\mathbf{5_2}$ were used. Thiol **4** was dissolved in borate buffer (50 mM, pH 8.2) at a concentration of 1.00 mM as stock solutions which could be diluted further for the kinetic measurement. Disulfide $\mathbf{5_2}$ was prepared by oxidizing a 1.00 mM solution of thiol **5** in borate buffer (50 mM, pH 8.2). The exchange reaction is overall second-order reaction[1]: first order each in thiol **4** and in disulfide $\mathbf{5_2}$. We analyzed the kinetics based on the reaction **4** + $\mathbf{5_2} \rightarrow$ **4-5** + **5**. We only measured the very early stage of the reaction, so that any subsequent exchange reactions (i.e. of **4** with heterodimer **4-5**) did not occur to a significant extent. We measured the kinetics using a stopped-flow setup equipped with a UV detector. The reaction was monitored at 320 nm, where the total absorbance is the sum of the absorbance of thiol **4**, **5** and disulfide $\mathbf{5_2}$ and **4-5**. The molar absorptivities of thiols **4** and **5** and disulfide $\mathbf{5_2}$ were determined as 1007 $M^{-1}cm^{-1}$ (R^2 = 0.9985), 16774 $M^{-1}cm^{-1}$ (R^2 = 0.9997) and 2850 $M^{-1}cm^{-1}$ (R^2 = 0.9559), respectively. Given the difficulty of obtaining pure heterodimer **4-5**, the molar absorptivity of dimer **4-5** was obtained indirectly using UPLC. Firstly, a mixture of disulfides $\mathbf{4_2}$, $\mathbf{5_2}$ and **4-5** was prepared in borate buffer (50 mM, pH 8.2) by mixing equimolar amounts of building blocks **4** and **5**, followed by air oxidation. The peak area of each of the three thiols was measured by UPLC. The molar absorptivity of **4-5** at 320 nm (3083 $M^{-1}cm^{-1}$) was then obtained from the mass balance using the previously determined molar absorptivities of $\mathbf{4_2}$ and $\mathbf{5_2}$. The rate constant for the disulfide exchange reaction was then obtained by analyzing the change in the concentration of **5** with time (Figure S16 and S17).

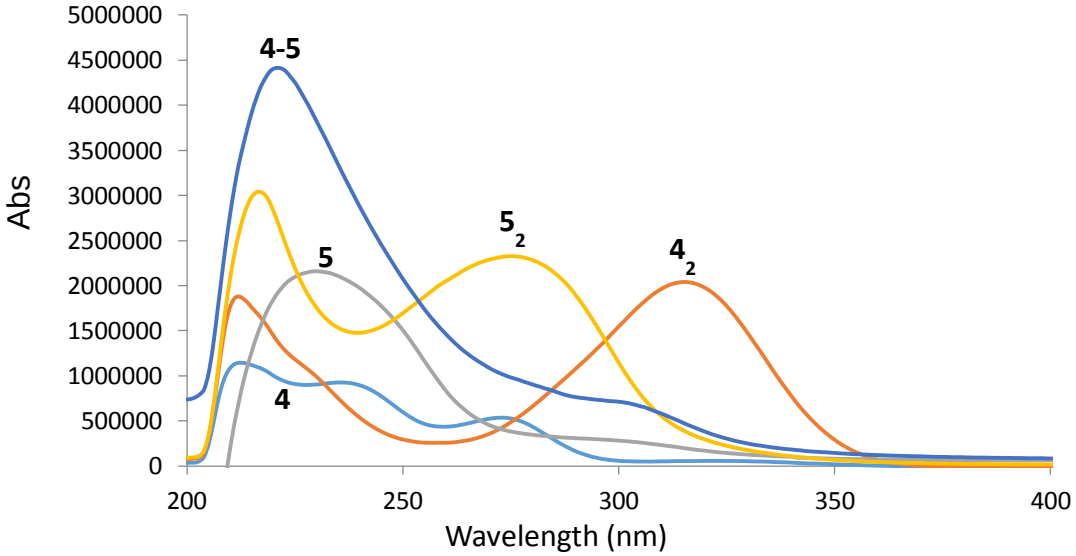

Figure S16. The UV spectra of thiol **4** (light blue), thiol **5** (gray), disulfide $\mathbf{4_2}$ (orange), disulfide $\mathbf{5_2}$ (yellow) and disulfide **4-5** (deep blue, from subtraction).

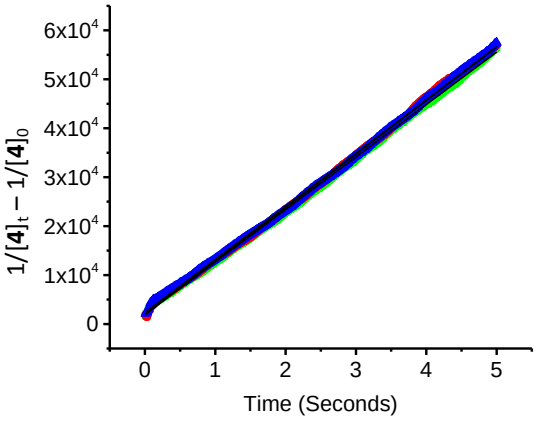

Figure S17. Kinetic data for the reaction of disulfide $\mathbf{5_2}$ with thiol 4. Three repeats of the same experiment are indicated in different colors and the curves fitted to the individual datasets are shown in black. The terms $[\mathbf{4}]_t$ and $[\mathbf{4}]_0$ refer to the concentration of thiol **4** at times t and t=0, respectively. The rate constant was obtained through fitting the data to a second order rate equation, yielding a value of 1.08 (±0.01) × 10^4 $M^{-1}s^{-1}$.

The concentrations of reactants used for measuring the rate constant were 0.010 mM in thiol and disulfide. The kinetics were followed using a stopped-flow

spectrophotometer in borate buffer (pH 8.2) at 25 °C. The reactions were monitored in triplicate for 5 seconds (sampling every 0.01 seconds).

S3.5 Selectivity of thiol oxidation and disulfide reduction with respect to replicator

In order to perform a reaction flux analysis the relative contributions of competing redox processes involving different species needed to be quantified. Two selectively factors *x* and *y* were defined for the reduction and oxidation processes, respectively. More specifically, *x* (ranging from 0-1) is defined as the fraction of the total consumed TCEP that reacts with hexamers exposed at the fiber ends (hexamers locked inside fibers are not reduced) when fiber ends and non-assembled macrocycles are present in equimolar quantities. The constant *y* (also ranging from 0-1) corresponds to the fraction of total consumed perborate that is used to convert monomer **1** into hexamers $\mathbf{1}_6$ at the fiber ends (any non-assembled hexamers are assumed to rapidly equilibrate to trimers and tetramers).

The value of *x* was determined by a competitive reduction experiment. Mixtures with equal amounts (0.095 mM in units of **1**) of $\mathbf{1}_6$ fibers and unassembled $\mathbf{1}_3$ and $\mathbf{1}_4$ were prepared by adding 12.5 μL $\mathbf{1}_6$ and $\mathbf{1}_3$/$\mathbf{1}_4$ (3.8 mM) into borate buffer with 1.5 M guanidinium chloride to a final volume of 500 μL. The samples were then reduced 8%, 20% and 40% by addition of the corresponding amounts of TCEP (from a 19 mM solution). UPLC was used to analyze the composition of the libraries immediately after reduction (Figure 3C). Given that previous work established that reduction of $\mathbf{1}_6$ occurs exclusively at the fiber ends[2], the data in this figure indicates that the fiber ends are remarkably fast to react (most likely as a result of electrostatically driven binding of TCEP to the $\mathbf{1}_6$ fibers). With an average fiber length of 100 nm and approximately 2 units of $\mathbf{1}_6$ per nm, only approximately 1% of $\mathbf{1}_6$ is exposed at the fiber ends. This approximation, combined with the data in the above figure, allowed us to estimate a value for *x* of 0.99.

The value of *y* was estimated by adding perborate to a solution of **1** and determining the product distribution by UPLC as soon as the perborate had all reacted (Figure S1B). This led to an estimate of *y* of 0.40.

S3.6 Summary of experimentally determined kinetic parameters

Table S3: Experimentally determined reaction orders, rate constants and flow rates used in the kinetic model of the fueled replication-destruction network.[a]

Process / parameter	**Order in reactant**	**Rate constant / flow (with different units)**	
Reduction by TCEP (k_{red})	1 (TCEP) 1 (disulfide)	1.11×10^5 M^{-1} s^{-1}	0.66×10^7 M^{-1} min^{-1}
Oxidation by perborate (k_{ox})	1 (perborate) 1 (thiol)	1.09 M^{-1} s^{-1}	65 M^{-1} min^{-1}
TCEP-perborate quenching (k_{quench})	1 (TCEP) 1 (perborate)	15 M^{-1} s^{-1}	900 M^{-1} min^{-1}
Thiol-disulfide exchange (k_X)	1 (thiol) 1 (disulfide)	1.08×10^4 M^{-1} s^{-1}	6.48×10^6 M^{-1} min^{-1}
TCEP and perborate flow		1.33×10^{-7} M s^{-1}	8×10^{-6} M min^{-1}
	Value		
x[b]	0.99		
y[c]	0.40		

[a] These data were obtained as described in sections S3.1-S3.5.

[b] *x* is the fraction of the total consumed TCEP that reacts with hexamers exposed at the fiber ends (hexamers locked inside fibers are not reduced) when fiber ends and non-assembled macrocycles are present in equimolar quantities.

[c] *y* is defined as the fraction of total consumed perborate that is used to convert monomer **1** into hexamers $\mathbf{1}_6$ at the fiber ends (any non-assembled hexamers are assumed to rapidly equilibrate to trimers and tetramers).

S4 Kinetic model and flux analysis

A deterministic model based on ordinary differential equations (ODEs) was developed to assess the fluxes through the different reaction channels in the complex reaction network. The model was developed in two stages. First, a partial model was developed for a system with only one replicator (the hexamer). Motivation for

developing the model for the hexamer was that this was the least reactive of the two replicators, so probing the extent to which the redox reagent acted on this species is important. In the second stage also the trimer was introduced that competes with the hexamer for the same building blocks.

S4.1 Partial model with only hexamer replicator

The model uses experimentally determined (see Section S3) reaction orders and rate constants for the oxidation of thiols by sodium perborate, the reduction of disulfides by TCEP, the exchange between thiols and disulfides, the quenching reaction between perborate and TCEP and the self-replication reaction. Also, the redox agent's selectivities were included in the model by two additional parameters, *x* and *y*, (defined in Section S3.5) as the relative selectivities towards replicators of the reducing and oxidizing agents, respectively. These experimental parameters are summarized in Table S3.

In addition, the model also includes rate constants for reaction steps associated with self-replication that are not readily obtained experimentally, including fiber nucleation, fiber elongation and fiber breakage. These rate constants were chosen such that the observed experimental behavior (length of the lag phase and shape of the sigmoidal growth of the replicator) is qualitatively reproduced (Table S4).

Table S4: Reaction orders and rate constants used in the kinetic model of the fueled replication-destruction network.

Process	Order in reactant	Rate constant
Oxidation by O_2 (k_{O2})	1	2×10^{-4} min^{-1}
Nucleation (k_N)	2 (3mers, 4mers)	1×10^{-6} M^{-1} min^{-1}
Catalysed elongation (k_{CE})	2 (3mers, 4mers) 1 (fibre ends)	1×10^{5} M^{-2} min^{-1}
Breakage (k_B^n)	1 (6mers)	$\begin{cases} 0 & n < 4 \\ exp\left(\frac{n}{1e1}\right)/1e4 & 4 \le n \le 200 \end{cases}$ min^{-1}
Inflow of $NaBO_3$		8×10^{-6} M min^{-1}
Inflow of TCEP		8×10^{-6} M min^{-1}

The model is constructed as a set of ordinary differential equations (ODEs) listed in Table S5. All concentrations are expressed in terms of units of building block **1**, so that mass balance is ensured without having to further consider stoichiometries for many of the reactions. By adhering to experimentally determined reaction orders the model remains physically realistic. In the model, monomer is oxidized to give linear dimer (Table S5 reactions 1 and 2), followed by trimer and tetramer rings (reactions 3 and 4.1). Trimer and tetramer can interconvert via disulfide exchange (reactions 5 and 6). The slow nucleation process, by which trimers (or tetramers) give rise to hexamer rings followed by hexamers assembling to forming new stacks (of the shortest length 2), is represented in the model by a single, slow, step (reaction 7 for trimer and 8 for tetramer). Also a stack's elongation is represented by a single step involving trimer (or tetramer) and the stack (reactions 9 and 10). The model also includes oxidation by $NaBO_3$ (reactions 2 and 4) and reduction by TCEP (reactions 13-15) as well as their inflow (reactions 16 and 17) and the direct reaction by $NaBO_3$ and TCEP (reaction 12).

Table S5: Reactions and rate equations considered in the kinetic model of replicating hexamer. Rate equations are given from the point of view of the reactants, and the ODEs are constructed using the equations and the stoichiometry of the reactions. Values of rate constants are given in Tables S3 and S4. $\mathbf{1}^{n}{}_{6}$ represents a stack of n hexamers (for example, the shortest stack of 2 hexamers is $\mathbf{1}^{2}{}_{6}$). All concentrations are expressed in terms of units of building block **1**, so, for example, $[\mathbf{1}^{n}{}_{6}]$ is the concentration of **1** that is contained in hexamer stacks of length n.

	Reaction	**Rate equation**
1	$\mathbf{1}_1 + ½O_2 \rightarrow \mathbf{1}_2$	$k_{O2}*[\mathbf{1}_1]$
2	$\mathbf{1}_1 + ½*NaBO_3 \rightarrow \mathbf{1}_2$	$k_{ox}*[\mathbf{1}_1]*[NaBO_3]$
3	$\mathbf{1}_2 + ½*O_2 \rightarrow \mathbf{1}_3$ $\mathbf{1}_2 + ½*O_2 \rightarrow \mathbf{1}_4$	$k_{O2}*[\mathbf{1}_2]$ $k_{O2}*[\mathbf{1}_2]$
4.1	$\mathbf{1}_2 + ½*NaBO_3 \rightarrow \mathbf{1}_3$ $\mathbf{1}_2 + ½*NaBO_3 \rightarrow \mathbf{1}_4$	$k_{ox}*(1-y)*[\mathbf{1}_2]*[NaBO_3]$ $k_{ox}*(1-y)*[\mathbf{1}_2]*[NaBO_3]$
4.2[a]	$\mathbf{1}_2 + ½*NaBO_3 \rightarrow \mathbf{1}_6$ $(n-1)*\mathbf{1}^{n-1}{}_6 + \mathbf{1}_6 \rightarrow n*\mathbf{1}^{n}{}_6$	$k_{ox}*y*[\mathbf{1}_2]*[NaBO_3]$ $k_{CE}*[\mathbf{1}_6]*[\mathbf{1}^{n-1}{}_6]/(n-1)$ {$n>2$}
5	$\mathbf{1}_3 + (\mathbf{1}_1+\mathbf{1}_2) \rightarrow \mathbf{1}_4$	$k_X*[\mathbf{1}_3]*([\mathbf{1}_1]+[\mathbf{1}_2])$
6	$\mathbf{1}_4 + (\mathbf{1}_1+\mathbf{1}_2) \rightarrow \mathbf{1}_3$	$k_X*[\mathbf{1}_4]*([\mathbf{1}_1]+[\mathbf{1}_2])$
7	$2*\mathbf{1}_3 \rightarrow 2*\mathbf{1}^{2}{}_6$	$k_N*[\mathbf{1}_3]^2$
8	$2*\mathbf{1}_4 \rightarrow 2*\mathbf{1}^{2}{}_6$	$k_N*[\mathbf{1}_4]^2$
9[a]	$(n-1)*\mathbf{1}^{n-1}{}_6 + \mathbf{1}_3 \rightarrow n*\mathbf{1}^{n}{}_6$	$k_{CE}*[\mathbf{1}_3]^2*[\mathbf{1}^{n-1}{}_6]/(n-1)$
10[a]	$(n-1)*\mathbf{1}^{n-1}{}_6 + \mathbf{1}_4 \rightarrow n*\mathbf{1}^{n}{}_6$	$k_{CE}*[\mathbf{1}_4]^2*[\mathbf{1}^{n-1}{}_6]/(n-1)$
11[a]	$n*\mathbf{1}^{n}{}_6 \rightarrow n*\mathbf{1}^{n/2}{}_6$	$k_B{}^n*[\mathbf{1}^{n}{}_6]/n$
12	$NaBO_3$ + TCEP $\rightarrow$ waste	$k_{quench}*[NaBO_3]*[TCEP]$

13	$\mathbf{1}_3$ + TCEP → $\mathbf{1}_1$	k_{red}*(1-x)*[$\mathbf{1}_3$]*[TCEP]
14	$\mathbf{1}_4$ + TCEP → $\mathbf{1}_1$	k_{red}*(1-x)*[$\mathbf{1}_4$]*[TCEP]
15[a]	n*$\mathbf{1}^n_6$ + TCEP → (n-1)*$\mathbf{1}^{n-1}_6$ + $\mathbf{1}_1$ 2*$\mathbf{1}^2_6$ + 2*TCEP → 2*$\mathbf{1}_1$	k_{red}*x*[TCEP]*[$\mathbf{1}^n_6$]/n k_{red}*x*[TCEP]*[$\mathbf{1}^2_6$]/2
16	$NaBO_3$ inflow	in_{NaBO3}
17	TCEP inflow	in_{TCEP}

[a] Because concentrations are expressed in terms of unit of building block **1**, reaction stoichiometries feature factors that correspond to the stack lengths. For example, elongating a stack of length n-1 with a single replicator macrocycle causes all n-1 macrocycles within the stack to transition into a stack of length n. For the same process the rate law features stack length in the denominator, since only the macrocycle at the stack end is determining the rate of the elongation reaction (the model assumes stacks grow only from one end).

The system was simulated deterministically using MATLAB's numerical integrator ode15s. Simulating the model with oxidation by O_2 until t = 20 days results in the transient formation of trimer and tetramer macrocycles that give way to hexamer replicator, which ultimately accounts for 98% of building block **1** (Figure S18). This behavior resembles qualitatively the typical kinetics of replicator emergence. Oxidation by O_2 is then switched off (by setting k_{O2} = 0) and an inflow of $NaBO_3$ and TCEP was commenced yielding a steady state value of 67% of the total material contained in $\mathbf{1}_6$ fibers under continued inflow of oxidant and reductant.

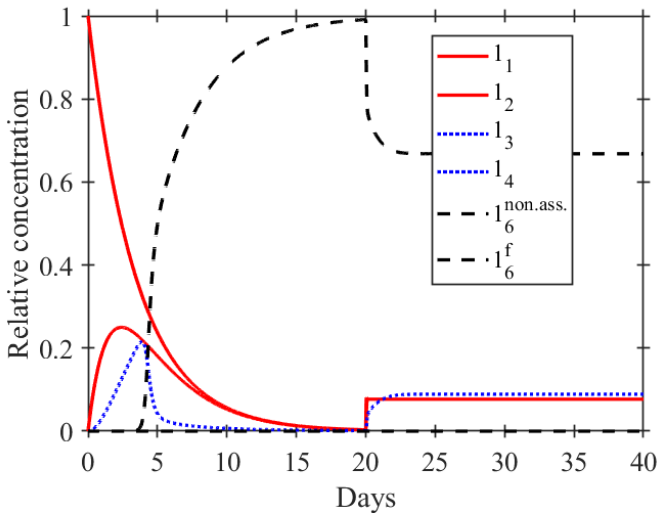

Figure S18. Simulation of the emergence of hexamer replicator, where $\mathbf{1}^f_6$, representing the sum of all stacked hexamers. At t = 0 the monomer concentration is 3.8×10^{-3} M. Until t = 20 days slow oxidation by oxygen took place. After 20 days the inflow of $NaBO_3$ and TCEP was started.

The fluxes of the oxidation and reduction reactions in the system were then analyzed. The redox reagents that are flown into the system act on replicator with a good efficiency. About 97% of the added TCEP reacts with the hexamer replicator (reaction 15); the remaining 3% represents reacts with the non-assembling macrocycles; mostly trimer and tetramer (reactions 13 and 14). Gratifyingly, the short-circuiting reaction (reaction 12) consumes less than 0.1% of the total redox reagents. This low flux is a consequence of the fact that perborate and TCEP do not reach very high concentrations as they react quickly with the thiols and disulfides, respectively, which are present at much higher concentrations. The different fluxes are shown graphically in Figure S19, in which the thickness of the arrows indicates the magnitude of the flux.

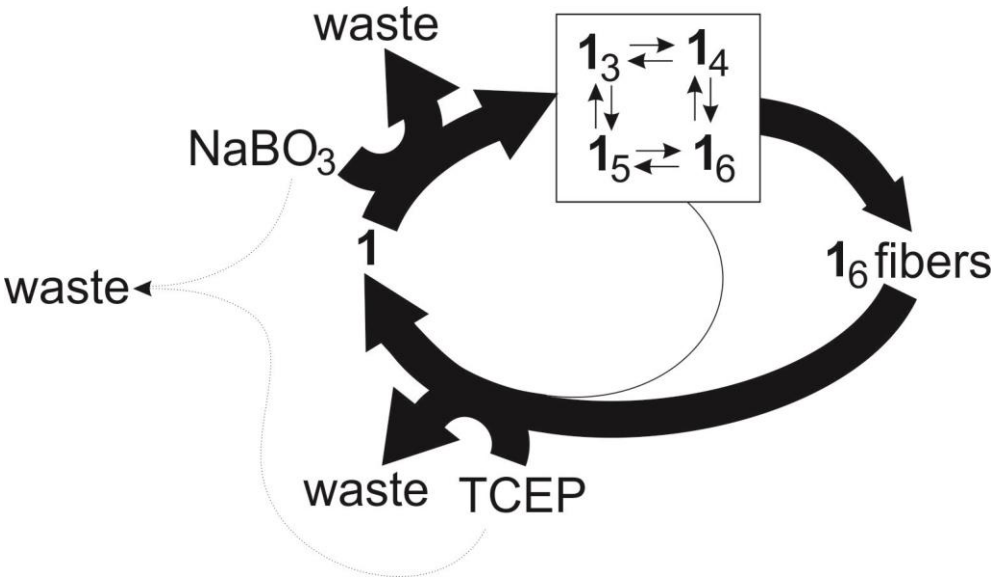

Figure S19. Graphical representation of the main fluxes through the simulated fueled replication-destruction system featuring only self-replication of $\mathbf{1}_6$.

S4.2 Full model with competing trimer and hexamer replicators

The partial model described in Section S4.1 was extended to include trimer replication via an elongation-breakage mechanism similar to that of the hexamers. The extended model consists of all the reactions listed in Table S5, together with the reactions in Table S6. All concentrations are expressed in terms of units of building block **1**, so that mass balance is ensured without having to further consider stoichiometries for many of the reactions. By adhering to experimentally determined reaction orders the model remains physically realistic.

Table S6: Reactions and rate equations added to the partial model to enable simulating the system of competing trimer and hexamer replicators. All concentrations are expressed in terms of units of building block **1**.

	Reaction	**Rate equation**
18	$2*\mathbf{1}_3 \rightarrow 2*\mathbf{1}^2{}_3$	$6*k_N*[\mathbf{1}_3]^2$
19	$2*\mathbf{1}_4 \rightarrow 2*\mathbf{1}^2{}_3$	$6*k_N*[\mathbf{1}_4]^2$
20[a]	$(n\text{-}1)*\mathbf{1}^{n-1}{}_3 + \mathbf{1}_3 \rightarrow n*\mathbf{1}^n{}_3$	$6*k_{CE}*[\mathbf{1}_3]^2*[\mathbf{1}^{n-1}{}_3]/(n\text{-}1)$
21[a]	$(n\text{-}1)*\mathbf{1}^{n-1}{}_3 + \mathbf{1}_4 \rightarrow n*\mathbf{1}^n{}_3$	$6*k_{CE}*[\mathbf{1}_4]^2*[\mathbf{1}^{n-1}{}_3]/(n\text{-}1)$
22[a]	$n*\mathbf{1}^n{}_3 \rightarrow n*\mathbf{1}^{n/2}{}_3$	$6*k_B{}^n*[\mathbf{1}^n{}_3]/n$
23[a]	$n*\mathbf{1}^n{}_3 + \text{TCEP} \rightarrow (n\text{-}1)*\mathbf{1}^{n-1}{}_3 + \mathbf{1}_1$ $2*\mathbf{1}^2{}_3 + 2*\text{TCEP} \rightarrow 2*\mathbf{1}_1$	$2*k_{red}*x*[\text{TCEP}]*[\mathbf{1}^n{}_3]/n$ $2*k_{red}*x*[\text{TCEP}]*[\mathbf{1}^2{}_3]/2$

[a] Because concentrations are expressed in terms of unit of building block **1**, reaction stoichiometries feature factors that correspond to the stack lengths. For example, elongating a stack of length *n*-1 with a single replicator macrocycle causes all *n*-1 macrocycles within the stack to transition into a stack of length *n*. For the same process the rate law features stack length in the denominator, since only the macrocycle at the stack end is determining the rate of the elongation reaction (the model assumes stacks grow only from one end).

Based on the experimental observation that the trimer replicator is reduced about twice as fast as hexamer replicator (as evident from Figure 3C) a factor 2 was added to the rate law of reaction 23 (Table S6). To reflect the fact that the trimer also replicates considerably faster than the hexamer a factor 6 was added in front of the rate laws of the processes related to trimer replicator (reactions 18-22 in Table S6). The factor 6 was selected as it resulted in a steady state similar to the experimentally observed one. Simulating this extended model with oxidation by O_2 (corresponding to the conditions in the experiment shown in Figure 2A of the main text) indeed results in trimers being the dominant product (accounting for 99% of the building block at t = 20 days; see Figure S20A).

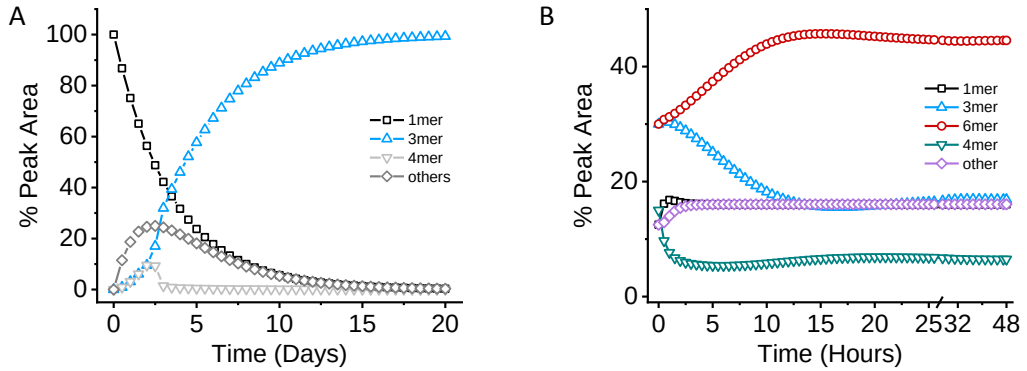

Figure S20. Modelling results obtained with the full model including trimer and hexamer replicator. (A) Kinetic modelling results corresponding to the experiment shown in Figure 2A in

which replicators emerge upon oxidation of building block **1** by oxygen from the air. Monomer **1** concentration at $t = 0$ was 3.8 mM. (B) Kinetic modelling results corresponding to the experiment shown Figure 4B in which a mixture of trimer and hexamer replicator is subjected to a continuous perborate/TCEP inflow that was maintained for the entire duration of the simulation.

We then modelled the experiment shown in Figure 4B in the main text, in which a 1:1 mixture of trimer and hexamer replicator (each quantified in number of units of building block **1**) is subjected to a continuous inflow of $NaBO_3$ and TCEP. The results are shown in Figure S20B and show that hexamer replicator now outcompetes the trimer replicator yielding a steady state enriched in the former.
We also compared the fluxes through the various reaction paths at the steady state (Table S7). The flux through the quenching reaction (number 12 in Table S5) is negligible compared to the flux involving thiols (numbers 2 and 4) or disulfides (numbers 13, 14 and 15).

Table S7: Reaction fluxes at steady state for the hexamer-only and the full model.

		Reaction flux (M min^{-1})	
	Reaction	**Hexamer-only**	**Full model**
2	$\mathbf{1}_1 + ½*NaBO_3 \rightarrow \mathbf{1}_2$	8.00×10^{-6}	8.00×10^{-6}
4.1	"$\mathbf{1}_2 + ½*NaBO_3 \rightarrow ½*\mathbf{1}_3 + ½*\mathbf{1}_4$"	4.80×10^{-6}	4.80×10^{-6}
4.2	$\mathbf{1}_2 + ½*NaBO_3 \rightarrow \mathbf{1}_6$	3.20×10^{-6}	3.20×10^{-6}
5	$\mathbf{1}_3 + (\mathbf{1}_1+\mathbf{1}_2) \rightarrow \mathbf{1}_4$	1.28	7.71×10^{-1}
6	$\mathbf{1}_4 + (\mathbf{1}_1+\mathbf{1}_2) \rightarrow \mathbf{1}_3$	1.28	7.71×10^{-1}
7	$2*\mathbf{1}_3 \rightarrow 2*\mathbf{1}^2_6$	1.14×10^{-13}	4.13×10^{-14}
8	$2*\mathbf{1}_4 \rightarrow 2*\mathbf{1}^2_6$	1.14×10^{-13}	4.13×10^{-14}
9	$(n\text{-}1)*\mathbf{1}^{n-1}_6 + \mathbf{1}_3 \rightarrow n*\mathbf{1}^n_6$	2.27×10^{-6}	8.19×10^{-7}
10	$(n\text{-}1)*\mathbf{1}^{n-1}_6 + \mathbf{1}_4 \rightarrow n*\mathbf{1}^n_6$	2.27×10^{-6}	8.19×10^{-7}
11	$n*\mathbf{1}^n_6 \rightarrow n*\mathbf{1}^{n/2}_6$	8.99×10^{-8}	7.46×10^{-8}
12	$NaBO_3 + TCEP \rightarrow$ waste	2.24×10^{-9}	1.39×10^{-9}
13	$\mathbf{1}_3 + TCEP \rightarrow \mathbf{1}_1$	1.32×10^{-7}	4.93×10^{-8}
14	$\mathbf{1}_4 + TCEP \rightarrow \mathbf{1}_1$	1.32×10^{-7}	4.93×10^{-8}
15	$n*\mathbf{1}^n_6 + TCEP \rightarrow (n\text{-}1)*\mathbf{1}^{n-1}_6 + \mathbf{1}_1$ $2*\mathbf{1}^2_6 + 2*TCEP \rightarrow 2*\mathbf{1}_1$	7.55×10^{-6} 8.99×10^{-8}	4.69×10^{-6} 7.46×10^{-8}
18	$2*\mathbf{1}_3 \rightarrow 2*\mathbf{1}^2_3$	N/A	2.48×10^{-13}
19	$2*\mathbf{1}_4 \rightarrow 2*\mathbf{1}^2_3$	N/A	2.48×10^{-13}
20	$(n\text{-}1)*\mathbf{1}^{n-1}_3 + \mathbf{1}_3 \rightarrow n*\mathbf{1}^n_3$	N/A	1.53×10^{-6}
21	$(n\text{-}1)*\mathbf{1}^{n-1}_3 + \mathbf{1}_4 \rightarrow n*\mathbf{1}^n_3$	N/A	1.53×10^{-6}
22	$n*\mathbf{1}^n_3 \rightarrow n*\mathbf{1}^{n/2}_3$	N/A	9.47×10^{-8}
23	$n*\mathbf{1}^n_3 + TCEP \rightarrow (n\text{-}1)*\mathbf{1}^{n-1}_3 + \mathbf{1}_1$ $2*\mathbf{1}^2_3 + 2*TCEP \rightarrow 2*\mathbf{1}_1$	N/A	2.87×10^{-6} 9.47×10^{-8}

In the full model featuring both trimer and hexamer replicator ca. 99% of the TCEP flown in is used to reduce the replicators (through reactions 15 and 23). The remaining ca. 1% is consumed through reduction of the non-assembled macrocycles; mostly trimer and tetramer (reactions 13 and 14). More of the flux now passes through the replicators, compared to the model in which only the hexamer replicator was present. This difference is consistent with the fact that the trimer replicator reacts faster with the redox reagents than the hexamer replicator. A graphical representation of the different fluxes is shown in Figure 1B.

S5. References

1. Singh, R., Whitesides, G.M. in *Patai's Chemistry of Functional Groups*, Patai, S., Rappoport, Z. Eds. (Wiley, 1993), Chapter 13.
2. Mattia, E., Pal, A., Leonetti, G., Otto, S. Mechanism of building block exchange in stacks of self-replicating macrocycles. *Synlett* **28**, 103-107 (2017).